NASA TECHNICAL NOTE

NASA TN D-2873

SEEDING CRITERION FOR NONEQUILIBRIUM MAGNETOHYDRODYNAMIC GENERATORS

by Frederic A. Lyman and Eli Reshotko

Lewis Research Center

Cleveland, Ohio

NATIONAL AERONAUTICS AND SPACE ADMINISTRATION • WASHINGTON, D. C. • JUNE 1965

NASA TN D-2873

SEEDING CRITERION FOR NONEQUILIBRIUM MAGNETOHYDRODYNAMIC GENERATORS

By Frederic A. Lyman and Eli Reshotko

Lewis Research Center
Cleveland, Ohio

NATIONAL AERONAUTICS AND SPACE ADMINISTRATION

For sale by the Clearinghouse for Federal Scientific and Technical Information
Springfield, Virginia 22151 – Price $3.00

SEEDING CRITERION FOR NONEQUILIBRIUM MAGNETOHYDRODYNAMIC GENERATORS*

by Frederic A. Lyman and Eli Reshotko

Lewis Research Center

SUMMARY

The various consequences of the addition of seed to a carrier gas in a magnetohydrodynamic (MHD) generator are examined. In particular, a criterion is established for determining whether the net effect of seed addition is to augment or decrease the power density in MHD generator channels that use magnetically induced nonequilibrium ionization. The analysis considers the effects of electron-neutral collisions, electron-ion collisions, ion slip, and variation of the electron energy loss factor with seed fraction and seed material. Included in the consideration of ion slip are the effects of seed fraction and seed material on ion-neutral collision frequency and on the relative drifts between seed ions and carrier ions.

The presented criterion is based on the determination of a break-even condition; namely, that combination of gas density, magnetic field, and induced voltage for which the power density of the unseeded carrier is neither augmented nor decreased by the addition of seed. The formulation is given in general terms and is applicable for arbitrary combinations of monatomic carrier and seed materials. The criterion may be separately applied to each successive station of a segmented-electrode Faraday generator.

Calculations of the break-even condition for various noble carrier gases with alkali seed have been performed and are presented in graphical form. The results indicate that ion slip very strongly affects the break-even conditions. Generally speaking, seeding is desirable, and the most beneficial effects are obtained for heavy seed materials.

INTRODUCTION

One of the key factors in obtaining high power density in magnetohydrodynamic (MHD) power generators is the achievement of high electric conductivity in the working

---

*The principal results of this investigation were reported at the ASME Winter Annual Meeting, New York City, Nov. 29-Dec. 4, 1964. The present report is a considerably expanded version of material which appeared as ASME Preprint 64-WA/ENER-10 under the title "Concerning the Need for Seeding in Nonequilibrium Magnetohydrodynamic Generator Channels."

fluid. In closed-cycle electric-power systems where seeded combustion plasmas are inapplicable, this problem is particularly severe because, at the highest working fluid temperatures currently contemplated for nuclear reactors or heat exchangers, the equilibrium electric conductivity of even a seeded gas is far below that required for a reasonable power density. A nonequilibrium means of obtaining high electric conductivity is accordingly of great interest.

The contemporary studies of nonequilibrium conductivity began with that of Kerrebrock (ref. 1). He considered the case of direct current gas discharges and showed that the electron temperature, at which the energy received by electrons from the electric field is balanced by that lost in collisions, can be considerably above the bulk gas temperature. He has in fact demonstrated the results to be well represented by a theory that assumes the ionization and recombination processes to be in equilibrium at the electron temperature so that the electron population is that corresponding to equilibrium at the electron temperature. The validity of Kerrebrock's hypothesis has been established for a cesium plasma by Ben Daniel and Tamor (ref. 2).

Hurwitz, Sutton, and Tamor (ref. 3) noted that the electron heating effect might also be obtained using the induced electric fields present in MHD generator channels. In their paper, as in Kerrebrock's analysis, the electron temperature was determined by balancing the energy gained by the electrons from the induced electric field with the energy lost by them in elastic collisions with the neutral atoms. They assumed that at the low degrees of ionization attained in generators, the electron-ion collisions would occur infrequently enough to be considered negligible.

Reference 4 showed, however, that at the elevated electron temperatures resulting from electron heating, a degree of ionization might be attained where the dominant process for momentum and energy exchange is electron-ion collisions. This was found to be particularly the case in noble gases displaying the Ramsauer effect. The addition of easily ionizable seed to a carrier gas has the two effects of (a) increasing the electron density of the working fluid and (b) increasing the electron energy losses through collision with seed atoms and ions, thus limiting the electron temperature. The first effect tends to augment the electric conductivity, while the second tends to decrease it. It was shown in reference 4 that in many cases for argon carrier gas with cesium seed the second effect was predominant, causing an overall reduction in electric conductivity. In fact, it was recommended in reference 4 that argon be used without seed as the working fluid in an MHD generator. This result is, however, sensitive to the values of the pertinent collision cross sections. The correct calculation of the electrical conductivity depends on the average rate of momentum transfer in collisions, which in turn requires the averaging of the momentum transfer rate over the velocity distributions of the colliding particles. In the previous investigations (refs. 1, 3, and 4), a value of the monoenergetic cross section corresponding to the average electron energy was chosen, which

is tantamount to ignoring the distribution of electron velocities. Furthermore, the prior investigations did not quantitatively consider the effect of the presence of both seed and carrier gas ions on ion slip.

It is the purpose of the present report to examine in an orderly manner the various consequences of the addition of seed to a carrier gas, including the aforementioned effects, and to establish a criterion to determine whether seed addition augments or decreases the power density. The formulated criterion may be separately applied to each successive station of a segmented electrode Faraday generator. The formulation is given in general terms and may be used for arbitrary combinations of monatomic carrier and seed materials.

ANALYSIS

The criterion mentioned in the INTRODUCTION will now be obtained. The basic idea is to determine the condition for which the addition of a vanishingly small amount of seed either increases or does not change the power density (power generated per unit volume). The condition for which the power density is unchanged by the addition of seed will be called the break-even point.

Basic Equations

In reference 4, Ohm's law and the electron energy equation are derived, including the effect of ion slip, for a slightly ionized gas containing only one type of ion (ions of the carrier gas). In the present report, it is necessary to include both carrier gas ions (c^+) and seed ions (s^+). (Symbols are defined in appendix A.) The details of the derivation are given in appendix B, where it is shown that all the basic equations of reference 4 still apply, provided that the definition of the ion-neutral collision frequency ν_{ia} is appropriately modified (see eq. (B19)).

The energy balance equation for the electrons is (ref. 4)

$$J^2 = 3\frac{e^2 k\delta}{m_c}(T_e - T)N_e^2 \tag{1}$$

where J is the current density, e is the electron charge, k is the Boltzmann constant, m_c is the mass of an atom of the carrier gas, T_e is the electron temperature, T is the static gas temperature, and N_e is the number density of electrons. The factor δ, which is sometimes called the mean loss factor, is a dimensionless quantity defined for

elastic collisions as

$$\delta \equiv \frac{\sum_{t \neq e} \frac{m_c}{m_t} \nu_{et}}{\sum_{t \neq e} \nu_{et}} \tag{2}$$

where the subscript t denotes each species of atom or ion that may be present, and ν_{et} is the average collision frequency for momentum transfer between the electrons and species t. The collision frequency is written

$$\nu_{et} = N_t \langle v_e \rangle Q_{et} \tag{3}$$

where $\langle v_e \rangle$ is the average thermal speed of the electrons

$$\langle v_e \rangle = \left(\frac{8kT_e}{\pi m_e} \right)^{1/2} \tag{4}$$

and Q_{et}, the average cross section for momentum transfer, is

$$Q_{et}(T_e) = \frac{4}{3} \left(\frac{m_e}{2kT_e} \right)^3 \int_0^\infty v_e^5 Q_m(v_e) \exp\left(-\frac{m_e v_e^2}{2kT_e} \right) dv_e \qquad (t = i, a) \tag{C11}$$

The quantity $Q_m(v_e)$ appearing in the integrand of equation (C11) is the momentum transfer cross section for a monoenergetic beam of electrons of speed v_e. Equation (C11) is the result of averaging the rate of momentum transfer in collisions over the velocity distributions of both the electrons and the species t of heavy particles (atoms or ions) in the manner described in appendix C. When the average momentum transfer cross section is calculated from equation (C11) for any one of the noble gases for some ranges of T_e, the result is found to be as much as an order of magnitude larger than the value of Q_m at beam energies equal to kT_e. The difference between $Q_{ec}(T_e)$ and Q_m is due to the large variation in Q_m with v_e for the noble gases displaying the Ramsauer effect. (If Q_m were independent of v_e, this difference would not be significant, since in that case $Q_{ec}(T_e) = (4/3)Q_m$.) Therefore, the use of the monoenergetic cross section instead of the average cross section, as was done in references 1, 3, and 4, can lead to significant errors.

For a segmented-electrode MHD generator, Ohm's law is (ref. 4)

$$J = \frac{\sigma_0}{1 + \beta_e \beta_i} uB(1 - K) \tag{5}$$

where u is the gas velocity, B is the intensity of the magnetic field (Wb/sq m), and K is the load parameter, which is the ratio of the actual voltage across the generator electrodes to the open-circuit voltage,

$$K \equiv \frac{E}{uB} \tag{6}$$

The conductivity σ_0 is

$$\sigma_0 = \frac{N_e e^2}{m_e \nu_e} \tag{7}$$

where

$$\nu_e = \sum_{t \neq e} \nu_{et} \tag{8}$$

is the total collision frequency for electrons. The electron Hall parameter β_e is defined as

$$\beta_e \equiv \frac{\omega_e}{\nu_e} \equiv \frac{eB}{m_e \nu_e} \tag{9}$$

where ω_e is the electron cyclotron frequency. The parameter β_i is

$$\beta_i \equiv \frac{\omega_i}{\nu_{ia}} \equiv \frac{2eB}{m_c \nu_{ia}} \tag{10}$$

where ν_{ia} is the effective ion-neutral collision frequency. The value of β_i is a measure of the slip of the ions through the neutral gas. The ion slip varies inversely with the gas density (through ν_{ia}) and directly with the magnetic field. The expression for ν_{ia} is derived in appendix B (see eq. (B19)).

The power density for the segmented electrode generator is[1]

$$P = JE = N_e \sqrt{\frac{3e^2 k\delta}{m_c}} (T_e - T) KuB \tag{11}$$

The seed fraction s, defined as

$$s \equiv \frac{N_s^o}{N_c^o} \tag{12}$$

is the parameter of main interest. The number densities of seed and carrier gases in the absence of ionization are denoted as N_s^o and N_c^o, respectively, where

$$N_s^o = N_s + N_{s^+} \tag{13}$$

$$N_c^o = N_c + N_{c^+} \tag{14}$$

The degrees of ionization of the seed and carrier gas are

$$x_c \equiv \frac{N_{c^+}}{N_c^o} \tag{15}$$

$$x_s \equiv \frac{N_{s^+}}{N_s^o} \tag{16}$$

respectively. The condition of charge neutrality is

---

[1]This is equivalent to the conventional formula

$$P = \frac{\sigma_0 u^2 B^2 K(1 - K)}{1 + \beta_e \beta_i}$$

Equation (11) is more convenient for subsequent manipulations.

$$N_e = N_i = N_{s^+} + N_{c^+} = (x_c + sx_s)N_c^o \tag{17}$$

It is assumed that the various ion and atom populations are in equilibrium with the free electrons at the electron temperature T_e. Then the Saha equations (eqs. (4) and (5) of ref. 4) may be written for the seed as

$$\frac{(x_c + sx_s)x_s}{1 - x_s} = \frac{1}{N_c^o}\frac{2g_{s^+}}{g_s}\left(\frac{2\pi m_e kT_e}{h^2}\right)^{3/2} \exp\left(-\frac{eV_s}{kT_e}\right) \tag{18}$$

and for the carrier gas as

$$\frac{(x_c + sx_s)x_c}{1 - x_c} = \frac{1}{N_c^o}\frac{2g_{c^+}}{g_c}\left(\frac{2\pi m_e kT_e}{h^2}\right)^{3/2} \exp\left(-\frac{eV_c}{kT_e}\right) \tag{19}$$

where g_s and g_c are statistical weights for the ground states of the seed and carrier atoms, respectively, g_{s^+} and g_{c^+} are statistical weights of the ground states of the seed and carrier ions, respectively, and V_s and V_c are the first ionization potentials of the seed and carrier gas, respectively.

Condition for Operation Without Seed

The power density, current, conductivity, electron density, and temperature all depend on the seed fraction s. Suppose that the generator is operating without seed with a prescribed load parameter K, magnetic field B, and gas velocity u. The problem is to determine the direction in which the power density varies when a small amount of seed is added. For this the sign of dP/ds in the neighborhood of $s = 0$ must be determined. When $dP/ds = 0$, the break-even condition will be attained, and this condition will require a certain relation between the operating parameters.

With the aforementioned assumptions, the electric field E is fixed, and the fractional change in the power density caused by the addition of seed is, from equation (11),

$$\frac{1}{P}\frac{dP}{ds} = \frac{1}{J}\frac{dJ}{ds} = \frac{1}{N_e}\frac{dN_e}{ds} + \frac{1}{2}\frac{1}{T_e - T}\frac{dT_e}{ds} + \frac{1}{2\delta}\frac{d\delta}{ds} \tag{20}$$

From equations (1), (5), and (7), it follows that for fixed K, u, and B

$$\nu_e^2(1 + \beta_e\beta_i)^2(T_e - T)\delta = \text{const} \tag{21}$$

Logarithmic differentiation of equation (21) gives

$$\frac{2}{1 + \beta_e\beta_i}\left(\frac{1}{\nu_e}\frac{d\nu_e}{ds} - \beta_e\beta_i\frac{1}{\nu_{ia}}\frac{d\nu_{ia}}{ds}\right) + \frac{1}{T_e - T}\frac{dT_e}{ds} + \frac{1}{\delta}\frac{d\delta}{ds} = 0 \tag{22}$$

Since ν_e, ν_{ia}, and δ are known functions of s and $T_e(s)$, equation (22) may be used to determine dT_e/ds. Then the resulting expression for dT_e/ds can be substituted into equation (20) to yield an expression for dP/ds. The details of this derivation are given in appendix D, where it is shown that $dP/ds \leqq 0$ if

$$\begin{aligned}
&\beta_e\beta_i\left\{\frac{T_e}{T_e - T} + \Psi\left[(1 - x_c)\left(3 + \frac{2eV_c}{kT_e} + \frac{T_e}{T_e - T}\right) + \frac{T_e}{T_e - T}\right]\right. \\
&\qquad + x_c\left(3 + \frac{2eV_c}{kT_e} + \frac{T_e}{T_e - T}\right) + \left(1 - \frac{m_c}{m_s}\right)(1 - 2x_c)\left(\frac{3}{2} + \frac{eV_c}{kT_e}\right)\left.\frac{\nu_{ei}}{\nu_e}\right\} \\
&\qquad \leqq 3\frac{\nu_{ei}}{\nu_e} - \frac{\nu_{ec}}{\nu_e}\left[2n + 1 + \frac{T_e}{T_e - T} - x_c\left(3 + \frac{2eV_c}{kT_e} + \frac{T_e}{T_e - T}\right)\right] \\
&\qquad - \left(1 - \frac{m_c}{m_s}\right)\frac{\nu_{ei}}{\nu_e}\left\{3\left(1 - \frac{x_c}{2}\right)\frac{\nu_{ei}}{\nu_e} + \frac{\nu_{ec}}{\nu_e}\left[\frac{3}{2} + \frac{eV_c}{kT_e} - \left(1 - \frac{x_c}{2}\right)(2n + 1)\right]\right\}
\end{aligned} \tag{23}$$

The number n is simply the exponent in a semiempirical relation for the cross section $Q_{ec} \sim T_e^n$ for scattering of electrons by carrier gas atoms. Typically, n is of the order 1. The quantity Ψ, which is defined in equation (D18), is related to the difference in mobilities of the two ion species in the carrier gas.

The aforementioned relation (eq. (23)) is derived for the limit of zero seed. It has been assumed that as s approaches zero, the degree of ionization of the seed approaches one; hence, the ionization potential and cross section of the seed do not appear. From equations (18) and (19), it can be shown that for $s = 0$, $x_s \approx 1$ to a high degree of approximation.

The inequality (23) is an implicit relation between T_e, N_c^o, B, and T, which establishes a range of electron temperatures in which the power density is not increased by seeding. It is not possible to obtain an explicit relation, because the various terms of

equation (23) are not simple functions of T_e. It is convenient for calculational purposes to assign N_c^o, T_e, and T and to calculate $\beta_e\beta_i$, which is proportional to B^2. For fixed values of T_e and T, the limiting magnetic field is then calculated over the allowable range of gas densities N_c^o. From curves of B against N_c^o, the break-even value of N_c^o corresponding to any given magnetic field may be found for prescribed values of T_e and T.

The electron temperature is, of course, not an independent parameter, because it depends on the rate of Joule heating through equation (1). Thus it is necessary to establish whether or not any prescribed electron temperature is actually attainable. The criterion for this is the value of the gas velocity u required to produce a given electron temperature. The required gas velocity is obtained from the relation

$$uB(1 - K) = \frac{m_e}{e}\sqrt{\frac{3k}{m_c}}\,(1 + \beta_e\beta_i)\nu_e\sqrt{T_e - T} \tag{24}$$

which follows from equations (1), (5), and (7). (Note that $\delta = 1$ in the limit of zero seed.) Finally, the break-even condition is conveniently expressed as a family of curves of $uB(1 - K)$ against N_c^o for various values of B and T. In appendix E, a sample calculation is given in order to clarify the details of the calculational procedure.

RESULTS AND DISCUSSION

Although the break-even condition (the equality in relation (23)) is utilized in the manner just described to obtain numerical results, it is of interest to consider the simpler forms to which it reduces in special cases so that the physical meaning of the condition may become clearer.

Zero Ion Slip

A useful limiting case is that in which ion slip is neglected. Then $\beta_i = 0$, and the right side of relation (23) must also be zero. The break-even condition for zero ion slip is further simplified for small degrees of ionization. For this case ($x_c \ll 1$ and $s = 0$), equation (19) may be written

$$x_c = \frac{g(T_e)}{(N_c^o)^{1/2}} \tag{25}$$

where

$$g(T_e) \equiv \left(\frac{2g_{c^+}}{g_c}\right)^{1/2} \left(\frac{2\pi m_e k T_e}{h^2}\right)^{3/4} \exp\left(-\frac{eV_c}{2kT_e}\right) \tag{26}$$

From equations (3), (15), and (17), for $x_c << 1$,

$$\frac{\nu_{ei}}{\nu_{ec}} = \frac{x_c}{1 - x_c} \frac{Q_{ei}}{Q_{ec}} \approx x_c \frac{Q_{ei}}{Q_{ec}} \tag{27}$$

Thus, for $x_c << 1$ and $s = 0$, equation (23) yields the following quadratic equation for the ratio ν_{ec}/ν_{ei}:

$$a\left(\frac{\nu_{ec}}{\nu_{ei}}\right)^2 + b\left(\frac{\nu_{ec}}{\nu_{ei}}\right) - c \leqq 0 \tag{28}$$

where

$$a = 2n + 1 + \frac{T_e}{T_e - T} \tag{29a}$$

$$b = 2n + 1 + \frac{T_e}{T_e - T} - 3 + \left(1 - \frac{m_c}{m_s}\right)\left[\frac{3}{2} + \frac{eV_c}{kT_e} - (2n + 1)\right] - \frac{Q_{ec}}{Q_{ei}}\left(3 + \frac{2eV_c}{kT_e} + \frac{T_e}{T_e - T}\right) \tag{29b}$$

$$c = 3\frac{m_c}{m_s} + \frac{Q_{ec}}{Q_{ei}}\left(3 + \frac{2eV_c}{kT_e} + \frac{T_e}{T_e - T}\right) \tag{29c}$$

Break-even operation of course corresponds to the equality sign in the relation (28). Since a and c are positive, equation (28) has only one positive root, namely,

$$\left(\frac{\nu_{ec}}{\nu_{ei}}\right)_{lim} = \frac{\sqrt{b^2 + 4ac} - b}{2a} \tag{30}$$

The corresponding gas density is

$$\left(N_c^o\right)_{lim} = \left[\frac{g(T_e)Q_{ei}}{Q_{ec}}\left(\frac{\nu_{ec}}{\nu_{ei}}\right)_{lim}\right]^2 \tag{31}$$

which is the gas density for break-even operation with zero ion slip. At higher gas densities, $\nu_{ec}/\nu_{ei} > (\nu_{ec}/\nu_{ei})_{lim}$, and inequality (28) is not satisfied. Hence, seeding increases the power density. At gas densities below $(N_c^o)_{lim}$, seeding will decrease the power density. It is not difficult to understand why the ratio of collision frequencies is the critical parameter for break-even operation without seed. At gas densities larger than that given by equation (31), electron-atom collisions account for most of the resistivity of the gas. According to equations (3), (7), and (8), the conductivity in that case is proportional to the degree of ionization. Seeding would then increase the degree of ionization and therefore improve the conductivity and power. At gas densities lower than break-even, where ν_{ei} is much larger than ν_{ec}, the conductivity becomes independent of the electron density and increases with the electron temperature. In this case, the addition of seed would lower the electron temperature (cf. eq. (D21)) and consequently decrease the conductivity and power density more than could be offset by the ionization of the seed.

Equation (31) sets an upper limit on the gas density, above which the addition of seed will increase the power density. Strictly speaking, it is an implicit relation for $(N_c^o)_{lim}$, inasmuch as the gas density also enters into Q_{ei} through the term $\ln \Lambda$ (see eqs. (C19) and (C20)). Equation (31) is used in the following manner to establish the break-even condition for zero ion slip. The electron and gas temperatures are assigned, a value for $\ln \Lambda$ between 5 and 10 is assumed, and $(N_c^o)_{lim}$ is calculated from equation (31). The value of $\ln \Lambda$ is recomputed with this density, and the calculation is repeated a few times until it converges. The corresponding value of $uB(1 - K)$ is then calculated from equation (24). Appendix E contains a sample calculation.

The results of such a calculation are conveniently represented in a graph of the voltage $uB(1 - K)$ plotted against the gas density N_c^o. This form is convenient because the variation of the gas dynamic properties along a duct can easily be traced. For a constant velocity generator for which B and K are also constant, the state of the gas would be represented by a horizontal line, while a constant area generator with constant B and K would be represented on a log-log plot by a straight line of slope -1, since ρu is constant. In general, K is not constant, and the generator operating curve is not straight, as will be seen subsequently.

The zero-ion-slip break-even condition for some of the noble gases is shown in figure 1, where the atomic mass of the seed is assumed to be equal to that of the carrier gas in order to reduce the number of parameters. For some combinations of gas and seed such as argon and potassium or xenon and cesium, this is very nearly the case.

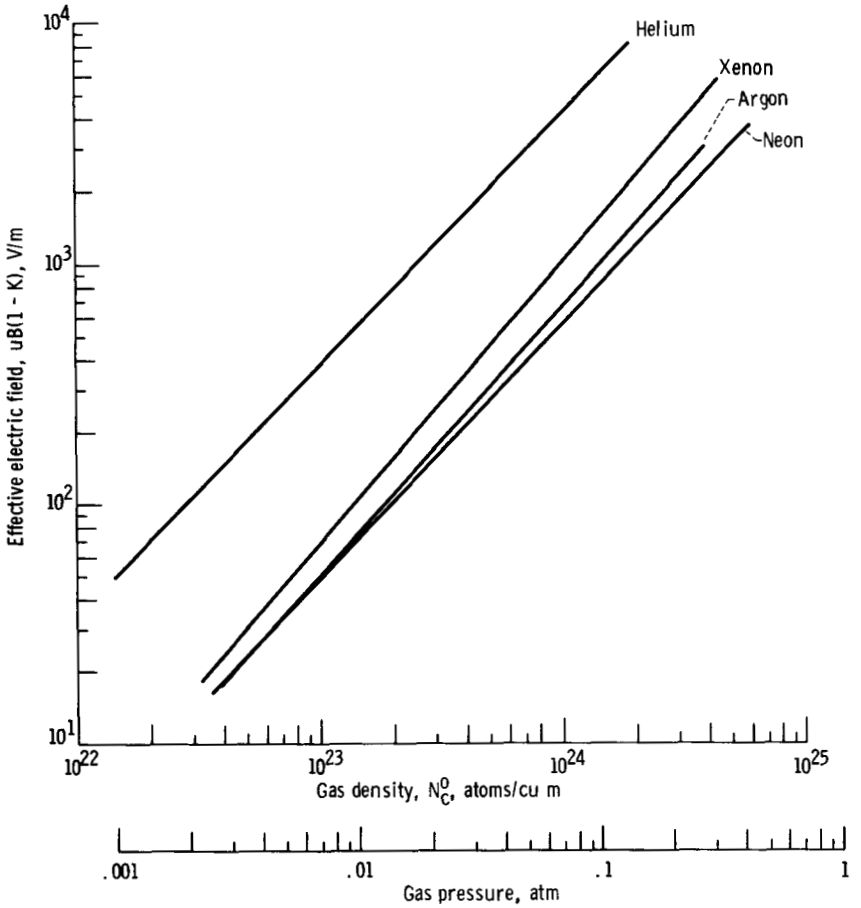

Figure 1. - Break-even curves for zero ion slip and equal atomic masses of carrier gas and seed. Static gas temperature, 500^0 K.

When $m_s = m_c$, $b = a - c$ and equation (30) becomes

$$\left(\frac{\nu_{ec}}{\nu_{ei}}\right)_{lim} = \frac{c}{a} \approx \frac{3}{2n + 1 + \dfrac{T_e}{T_e - T}} \tag{32}$$

since Q_{ec}/Q_{ei} is usually of the order 10^{-3}. Equation (32) can also be obtained quite directly from the right side of equation (23) by setting $m_c = m_s$ and $x_c \approx 0$. From equation (32), it is clear that the electron-ion and electron-atom collision frequencies are of the same order at break-even.

The break-even curves in figure 1 are for all practical purposes straight lines. There is no obvious reason why this should be so, but it is most likely due to the fact that the exponential variation of $g(T_e)$ in the formula for $(N_c^o)_{lim}$ (eq. (31)) is much more significant than the purely algebraic variation of the other terms. To the right of any one of these lines, $N_c^o > (N_c^o)_{lim}$, and the power density is increased by seeding, whereas

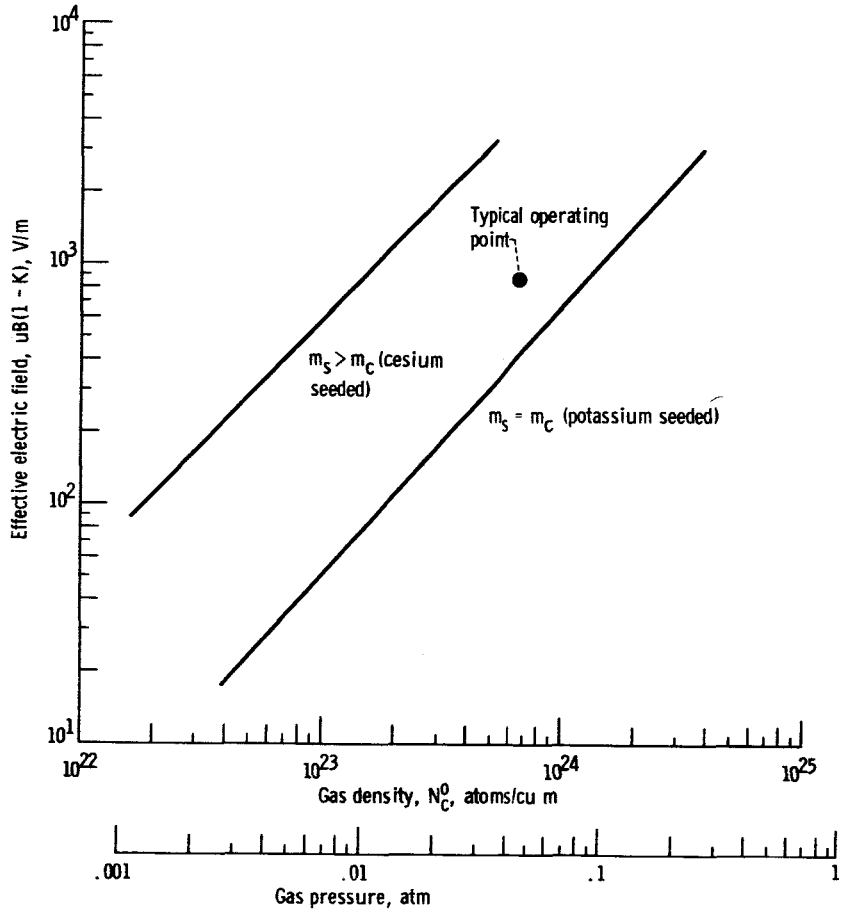

Figure 2. - Effect of seeding with material whose atomic mass is greater than that of carrier gas. Argon; static gas temperature, 500° K.

seeding decreases the power density to the left of the line.

There is no easily discernible pattern in the location of the break-even curves for different gases. It is evident from equations (31) and (26) that for a given electron temperature $(N_c^o)_{lim}$ will increase exponentially with decreasing ionization potential and varies as the inverse square of the cross section Q_{ec}. Furthermore, uB(1 - K) is proportional to Q_{ec}, since in the present case $\nu_e \approx \nu_{ec}(1 + a/c)$. Therefore the break-even curve for the gas with the lowest ionization potential should be closest to the lower right corner of the graph. Unfortunately, for the noble gases a low ionization potential does not go hand in hand with a low electron scattering cross section. In fact xenon, which has the lowest ionization potential, has one of the highest cross sections. The conflicting requirements on the ionization potential and cross section are responsible for the location of the curves shown in figure 1.

The obvious way to use the curves of figure 1 is to choose a particular gas and the values of the operating parameters u, B, K, and N_c^o and to decide whether seeding is required by where the point representing the operating condition falls relative to the

break-even curve. If the break-even curve is below the operating point, addition of seed with atomic mass equal to that of the carrier gas will decrease the power density; however, the addition of seed with atomic mass different from that of the carrier gas may move the break-even curve to the other side of the operating point, which indicates that such seed will increase the power density. Examination of equations (28) to (30) shows that if the seed atoms are heavier than the carrier gas atoms, then the ratio $(\nu_{ec}/\nu_{ei})_{lim}$ and $(N_c^o)_{lim}$ are decreased and the break-even curve is moved to the left. This behavior may be accounted for by the behavior of the elastic loss factor δ defined by equation (2). If $m_s > m_c$, then the addition of seed decreases δ. Figure 2 illustrates this effect when argon (atomic weight, 39.944) is seeded with cesium (atomic weight, 132.91).

Effect of Ion Slip

For $\beta_i \neq 0$ the break-even condition is evaluated numerically, as described previously and in appendix E. It is instructive to consider first the simplest case, where both the atomic masses and the mobilities of the seed and carrier gas are equal. In this case, the loss factor δ is unchanged by the addition of seed; and the quantity Ψ, representing the difference in ion mobilities, vanishes. The break-even condition becomes

$$\beta_e\beta_i = \frac{3\dfrac{\nu_{ei}}{\nu_e} - \dfrac{\nu_{ec}}{\nu_e}\left[2n + 1 + \dfrac{T_e}{T_e - T} - x_c\left(3 + \dfrac{2eV_c}{kT_e} + \dfrac{T_e}{T_e - T}\right)\right]}{\dfrac{T_e}{T_e - T} + x_c\left(3 + \dfrac{2eV_c}{kT_e} + \dfrac{T_e}{T_e - T}\right)} \tag{33}$$

When $N_c^o = (N_c^o)_{lim}$, as defined in equation (31), the numerator vanishes and $\beta_e\beta_i = 0$. Suppose that for a fixed T_e, N_c^o is continually decreased below $(N_c^o)_{lim}$. It is clear from equations (25) and (27) that the degree of ionization will then increase, as will the ratio ν_{ei}/ν_{ec}. Therefore, $\beta_e\beta_i$ will increase with decreasing N_c^o. (The term containing x_c in the denominator is generally of less importance for small x_c.) Physically, the increase in $\beta_e\beta_i$ is due to an increase in ion slip. Because of the lower gas density, ion-neutral collisions become less frequent, and the mechanism for extracting part of the mechanical energy from the gas and using it to Joule heat the electrons becomes less effective. As shown in figure 3, the effective electric field $uB(1 - K)$ required for electron heating is everywhere above that for $\beta_e\beta_i = 0$, the difference between the curves increasing as $\beta_e\beta_i$ increases (see eq. (24)). This difference becomes large enough to

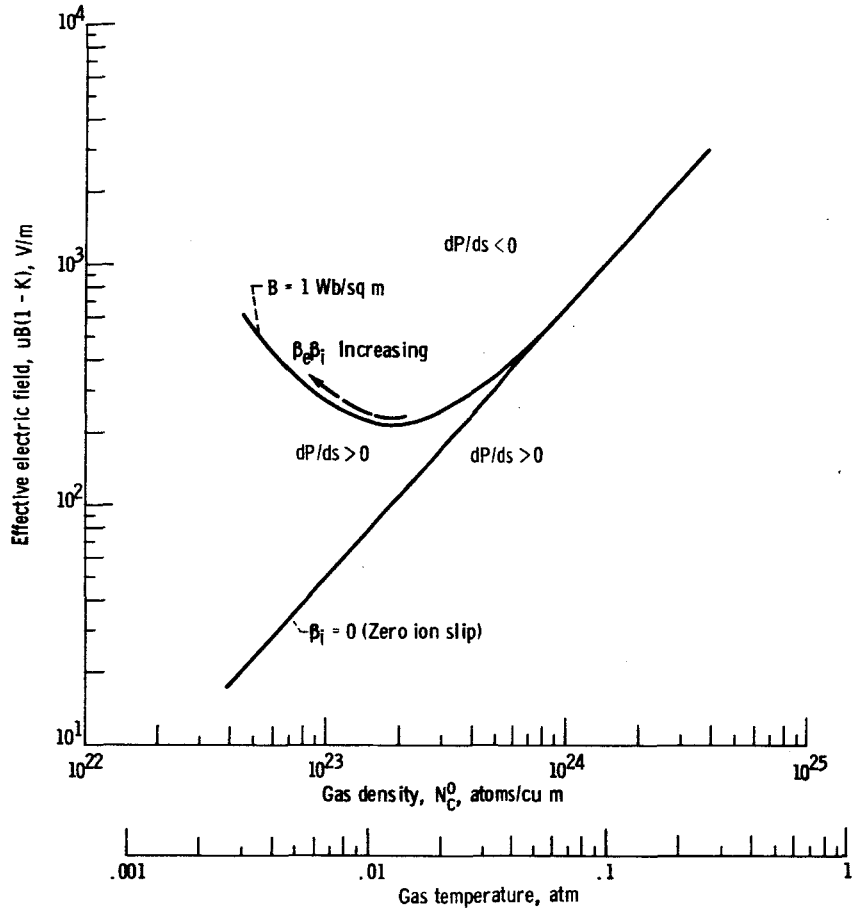

Figure 3. - Effect of ion slip on break-even curve for argon. Static gas temperature, 500^0 K; $m_s = m_c$; equal ion mobilities.

turn the break-even curve upward at low density. The range of parameters over which seeding is advantageous is increased, since $dP/ds > 0$ everywhere below the break-even curve.

For unequal atomic masses and mobilities of seed and carrier gases, the situation changes markedly from that of the preceding example, because the variations of the loss factor δ and of the effective ion-neutral collision frequency ν_{ia} become appreciable. This can be ascertained from the numerical magnitudes of the second and fourth terms on the left side of equation (23), since $eV_c/kT_e >> 1$. Because the general break-even condition is quite sensitive to the ratios of ion mobilities and atomic masses of the seed and carrier, as well as to the cross section and ionization potential of the carrier, it is difficult to draw general conclusions from equation (23). Each combination of seed and carrier must be considered separately. The results are shown in figures 4 to 9 for a static gas temperature of 500^0 K (which is typical of supersonic generators) and for various magnetic fields. Figure 4, for cesium-seeded argon, and figure 9, for cesium-seeded helium, are of a different character than figures 5 to 8. The break-even curve

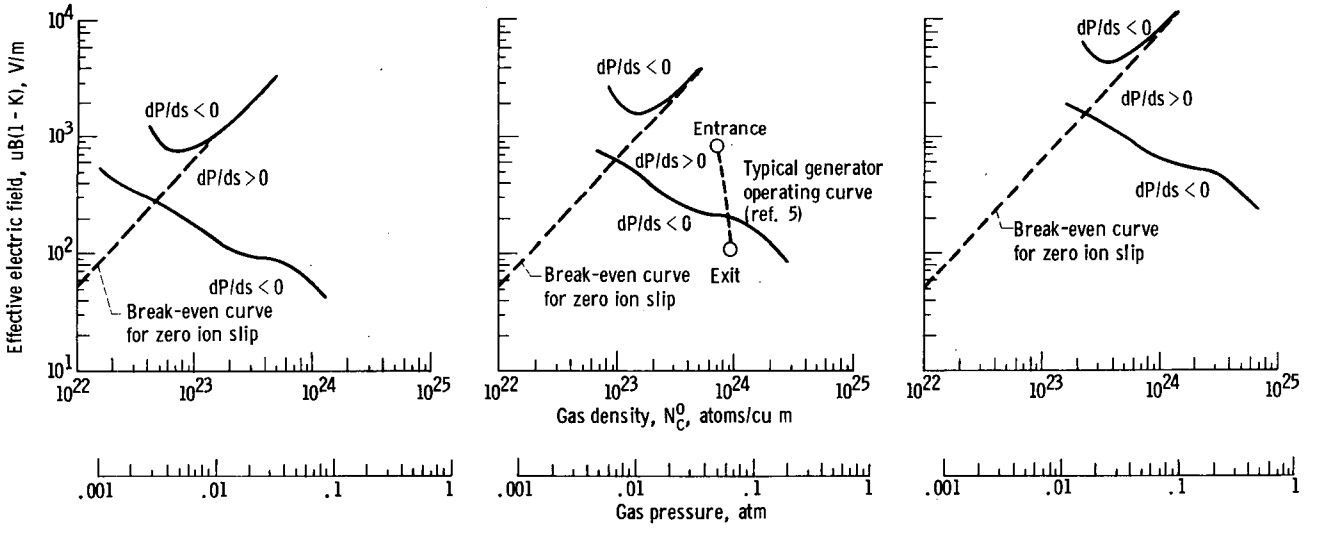

(a) Magnetic field strength, 1 weber per square meter.

(b) Magnetic field strength, 2 webers per square meter.

(c) Magnetic field strength, 5 webers per square meter.

Figure 4. - Break-even curves for cesium-seeded argon. Static gas temperature, 500° K.

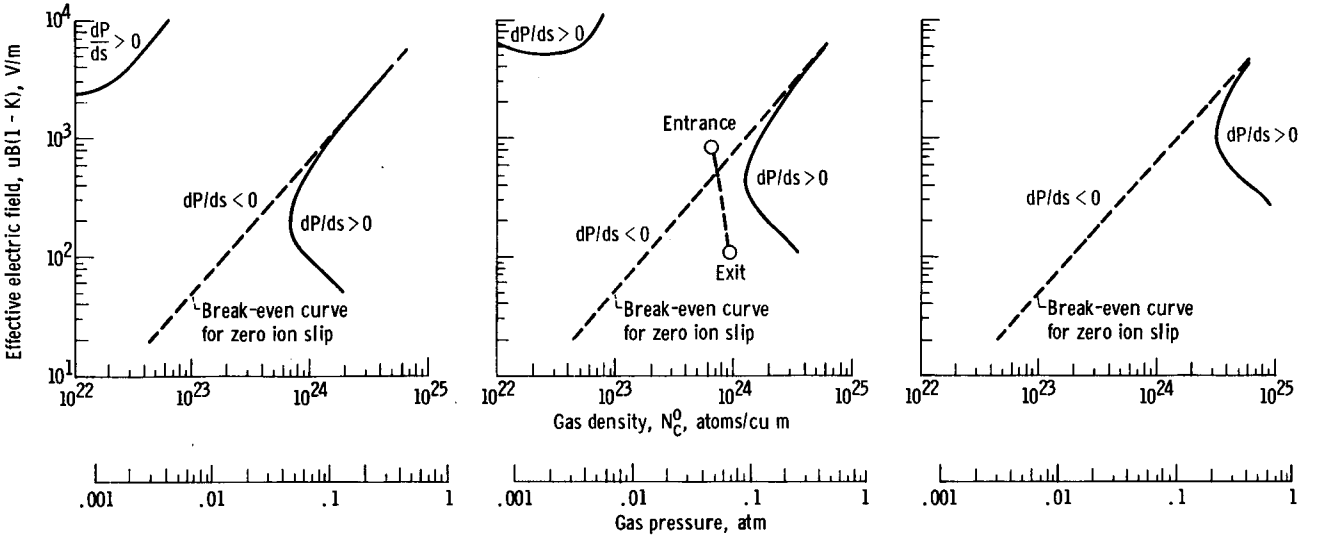

(a) Magnetic field strength, 1 weber per square meter.

(b) Magnetic field strength, 2 webers per square meter.

(c) Magnetic field strength, 5 webers per square meter.

Figure 5. - Break-even curves for potassium-seeded argon. Static gas temperature, 500° K.

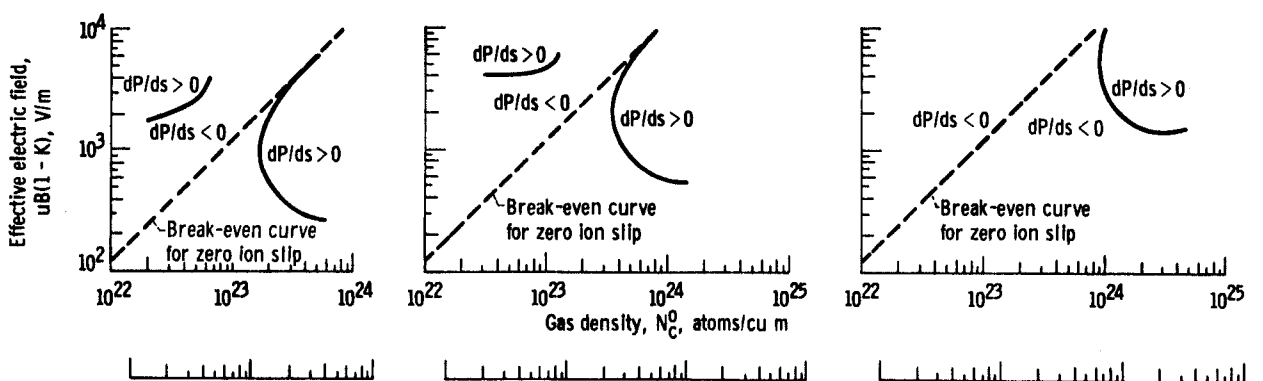

(a) Magnetic field strength, 1 weber per square meter.

(b) Magnetic field strength, 2 webers per square meter.

(c) Magnetic field strength, 5 webers per square meter.

Figure 6. - Break-even curves for cesium-seeded neon. Static gas temperature, 500° K.

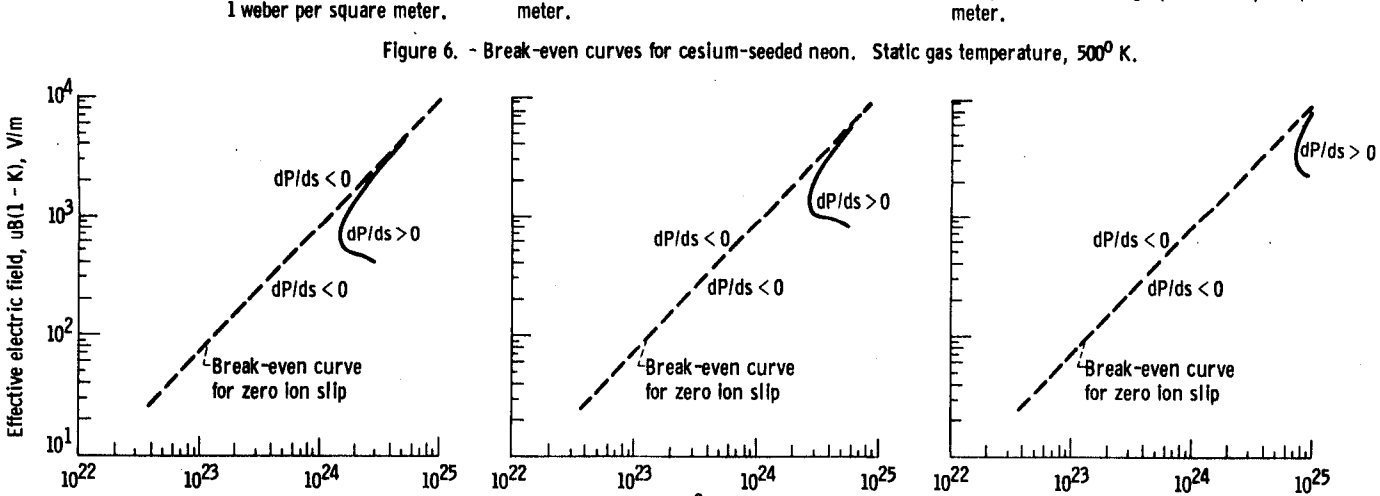

(a) Magnetic field strength, 1 weber per square meter.

(b) Magnetic field strength, 2 webers per square meter.

(c) Magnetic field strength, 5 webers per square meter.

Figure 7. - Break-even curves for sodium-seeded neon. Static gas temperature, 500° K.

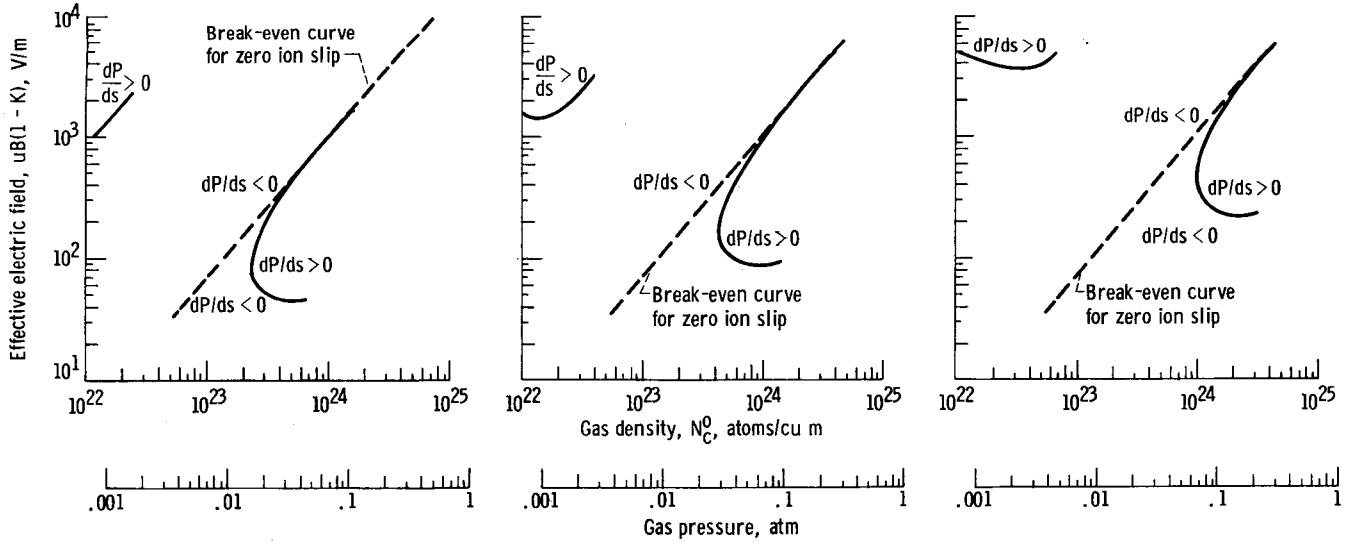

(a) Magnetic field strength, 1 weber per square meter.

(b) Magnetic field strength, 2 webers per square meter.

(c) Magnetic field strength, 5 webers per square meter.

Figure 8. - Break-even curves for cesium-seeded xenon. Static gas temperature, 500° K.

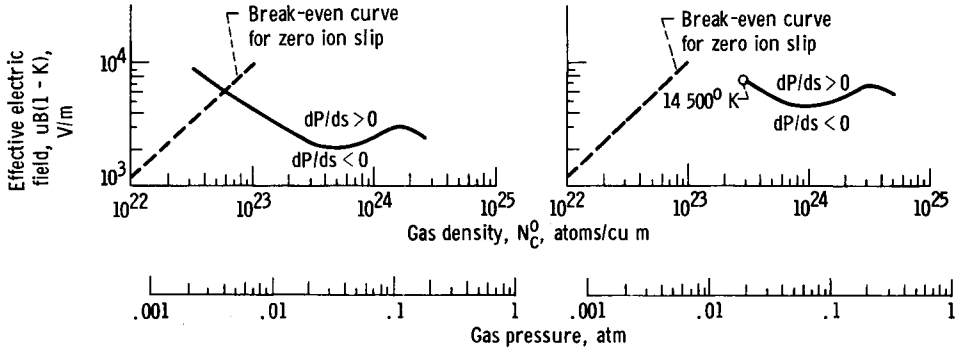

(a) Magnetic field strength, 1 weber per square meter.

(b) Magnetic field strength, 2 webers per square meter.

Figure 9. - Break-even curves for cesium-seeded helium. Static gas temperature, 500° K.

of figure 4 has an upper and a lower branch corresponding to high or low electron temperatures, respectively. In the regions above the upper branch and below the lower branch, seeding decreases the power density, while between the branches seeding increases the power density. The upper branch is similar to the curve of figure 3 and may be interpreted physically in the same way. In the region below the lower curve, the electron temperature is low and collisions of electrons with carrier gas atoms limit the conductivity. The addition of very small amounts of seed changes the conductivity only slightly, but because the seed ions are more mobile than ions of the carrier gas, seeding causes ion slip to increase more rapidly than the conductivity, which causes the factor $\sigma_0/(1 + \beta_e\beta_i)$ in the power density to decrease. Although seeding is not required in the region below the lower branch, this region is of little practical significance because of the low electron temperature and consequently the small degree of ionization and low power density.

The break-even curves of figures 5 to 8 have also two branches. The upper branch corresponds to high electron temperatures and low gas densities (this branch is not shown in figs. 5(c), 6(c), and 7, since it falls outside the range of electric fields and gas densities of interest). The lower branch, corresponding to higher gas densities and lower electron temperatures, is below and to the right of the break-even line for zero ion slip. Instead of crossing the zero ion slip line, as in figures 4 and 9, this lower branch becomes tangent to it. The different character of the break-even curves of figures 5 to 8 from those of figures 4 and 9 is due to the variation in the mobilities of carrier and seed ions among the various combinations of carrier and seed.

Seeding increases the power density in two regions of figures 5 to 8, above the upper branch, and to the right of the lower branch. In the first region, the effective electric field $uB(1 - K)$ is generally too high to be attained in practice. The range of gas densities and field strengths in the second region are of more practical interest.

A typical generator operating curve is indicated by the short dashed curve in figures 4(b) and 5(b) for argon. The generator operating conditions are taken from one of the cases that was extensively investigated in reference 5. In that reference the one-dimensional MHD equations were solved for a constant-area channel, where the nonequilibrium conductivities of seeded rare gases were calculated on the same basis as they are herein. The electric field E was taken to be constant in reference 5, as required by Maxwell's equation for the assumed one-dimensional situation. Since the gas velocity varies along the generator duct, for this case it is convenient to define a new constant load parameter K_1 as

$$K_1 = \frac{E}{u_1 B} \tag{34}$$

where u_1 is the gas velocity at the entrance section. When this definition is combined with conservation of mass, $\rho u = \rho_1 u_1$, the following equation for the operating curve is obtained:

$$uB(1 - K) = u_1 B \left(\frac{\rho_1}{\rho} - K_1 \right) \tag{35}$$

The dashed curves shown in figures 4(b) and 5(b) are for an entrance Mach number of 3.0 and an entrance stagnation temperature of 4000° R (2222° K), for which the entrance gas velocity u_1 is 1316 meters per second. For a magnetic field strength of 2 webers per square meter, a stagnation pressure of 1.64×10^5 newtons per square meter (1.62 atm) yields the optimum power density (ref. 5). The same conditions are assumed herein. In this case it can be seen that the addition of cesium will increase the power density except at the very end of the operating line. This conclusion is in agreement with reference 5, in which the addition of a very small amount of cesium seed (s = 0.000366) to argon carrier gas was found to yield the optimum total power output. Figure 5(b) shows that seeding with potassium is detrimental to the power density throughout the generator. Potassium seed was found to be inferior to cesium in reference 5, but potassium-seeded argon still produced a higher total power than unseeded argon. The mobility of ions, however, was calculated on the basis of the polarizability of the carrier gas atoms in reference 5. Such a calculation gives equal mobilities of argon and potassium ions in argon, whereas the mobility of argon ions in argon is less than that of potassium ions in argon because of charge exchange. Inclusion of charge exchange in this report accounts for the difference in conclusions regarding seeding of argon with potassium.

The upper limit on the gas velocity is

$$u_{max} = \sqrt{2 c_p T_0} \tag{36}$$

where $c_p = \frac{5}{2} \frac{k}{m_c}$ is the constant pressure specific heat and T_0 is the stagnation temperature. The values of u_{max} are useful in interpreting the results and are given in table I. The maximum attainable electric field and voltage may be estimated from these values of u_{max} and the magnitude of the available magnetic field. At the present time, a magnetic field of 2 webers per

TABLE I. - MAXIMUM GAS VELOCITIES

Gas	Stagnation temperature, T_0, $^{\circ}$K			
	1500	2000	2500	3000
	Maximum gas velocity, m/sec			
Helium	3947	4558	5096	5582
Neon	1758	2030	2270	2486
Argon	1250	1443	1613	1767
Xenon	689	796	890	975

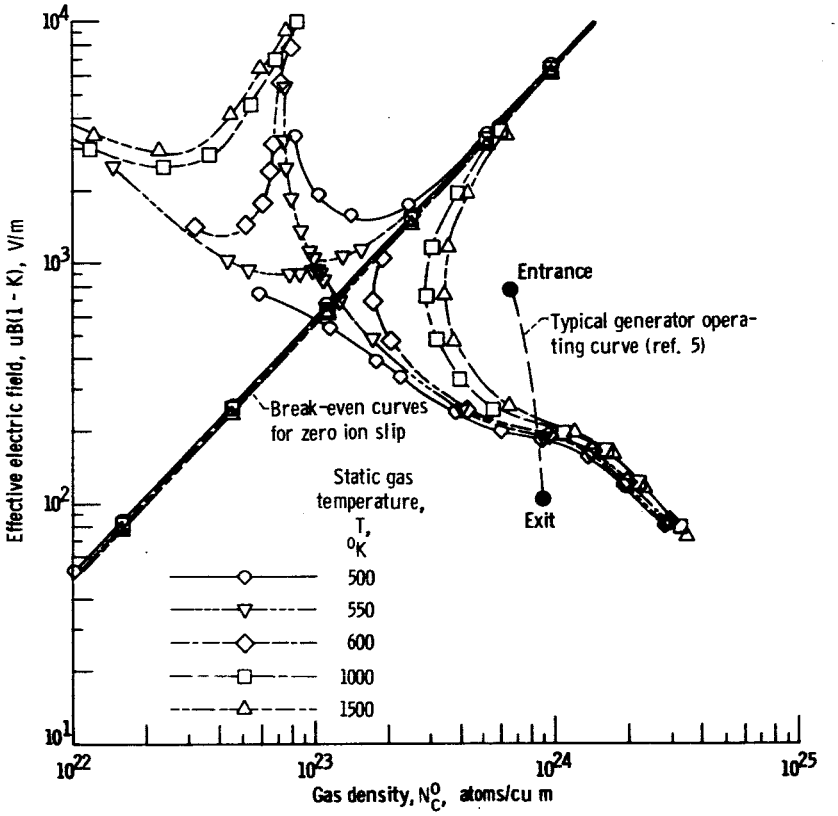

Figure 10. - Effect of gas temperature on break-even curves for cesium-seeded argon. Magnetic field strength, 2 webers per square meter.

square meter (20 000 G) is typical of MHD generators. For this magnetic field and K = 0.5, the maximum attainable field uB(1 - K) is equal to u_{max} in magnitude and is of the order of 10^3 volts per meter. With a very high magnetic field, say B = 10 webers per square meter (100 000 G), the magnitude of uB(1 - K) may reach 10^4.

Effect of Static Temperature

In figures 1 to 9 the gas temperature was taken to be 500° K, a typical value for supersonic generator. The effect of changing the gas temperature from 500° to 1500° K is shown in figure 10. The break-even curves for zero ion slip are very slightly affected by the gas temperature. However, the character of the curves for $\beta_i \neq 0$ varies significantly with gas temperature in the range from 500° to 600° K; and in fact, for gas temperatures of 600° K and higher, the break-even curves for cesium-seeded argon have the same character as the curves for the other combinations of gas and seed at 500° K shown in figures 5 to 8. Since there is insignificant variation of the alkali ion mobilities in the noble gases with temperature, the change in the character of the break-even curves that accompanies a change in gas temperature is due to the variation of the

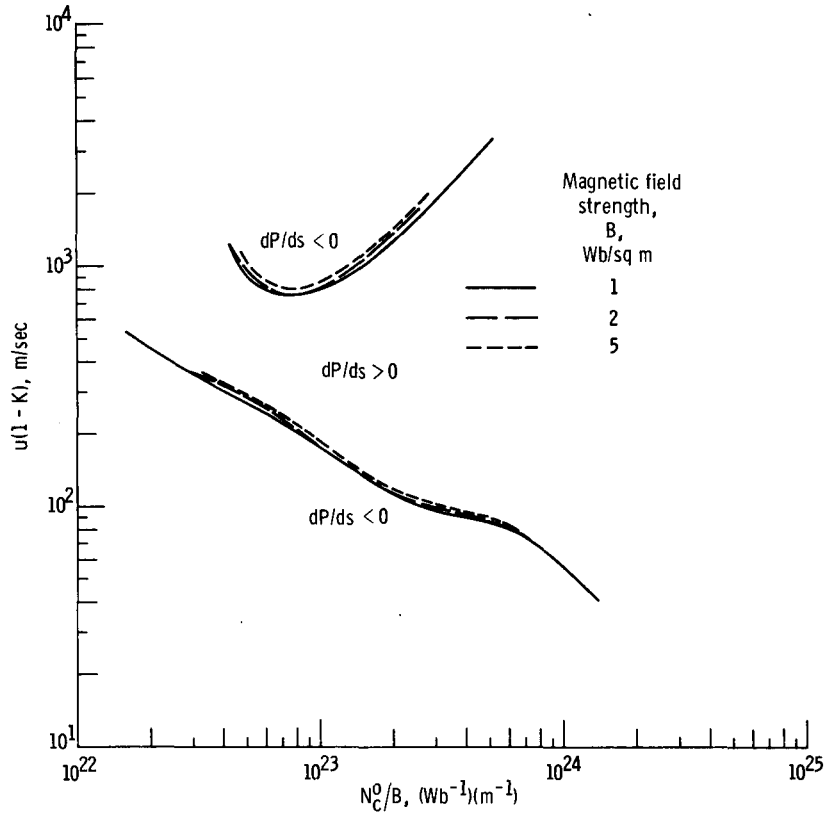

Figure 11. - Correlation of break-even curves when plotted as function of N_c^o/B for cesium-seeded argon. Static gas temperature, 500^o K.

mobility of the carrier ions with temperature, caused by charge exchange (see the discussion in appendix E).

Effect of Magnetic Field

Finally, it is interesting to note that the break-even curves for various magnetic fields fall rather close together when u(1 - K) is plotted against N_c^o/B, as shown in figure 11 for a constant gas temperature of 500^o K. This fact may be used to estimate roughly the location of the break-even curves for various magnetic fields when the shape of the curve for one magnetic field is known.

GENERATOR PERFORMANCE WITH UNSEEDED GASES

The purpose of the preceding analysis was to establish the regions of operation of a generator where the addition of alkali seed to a given noble carrier gas would increase the power density. A comparison of various combinations of seed and carrier gases re-

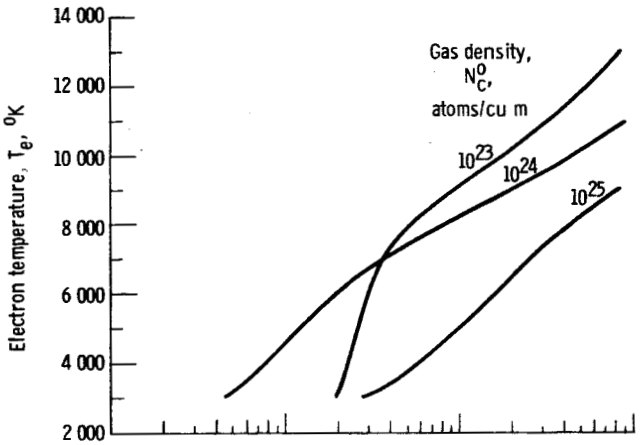

(a) Electron temperature against effective electric field.

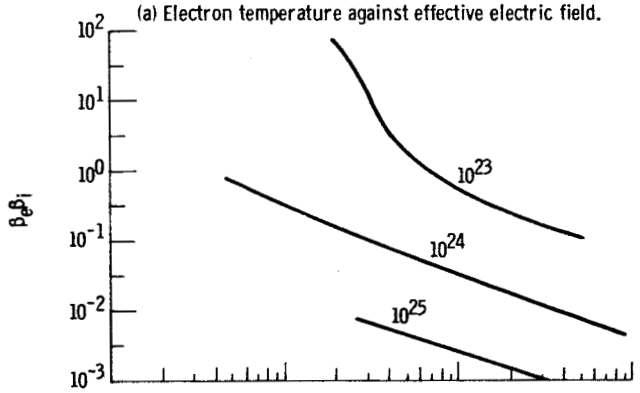

(b) $\beta_e\beta_i$ against effective electric field.

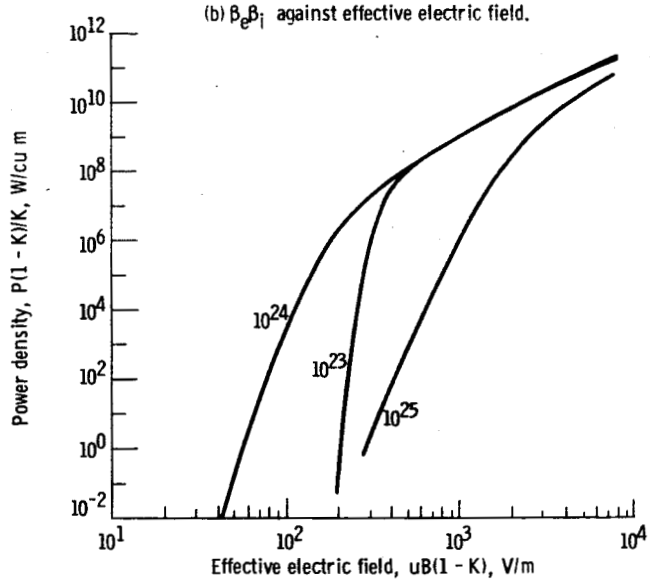

(c) Power density against effective electric field.

Figure 12. - Performance parameters as functions of electric field for unseeded argon. Magnetic field strength, 2 webers per square meter; static gas temperature, 500^0 K.

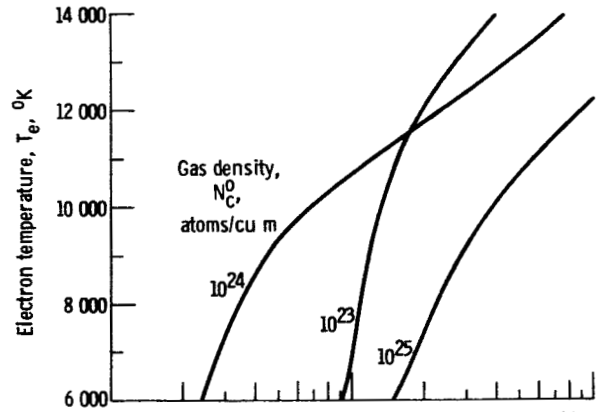

(a) Electron temperature against effective electric field.

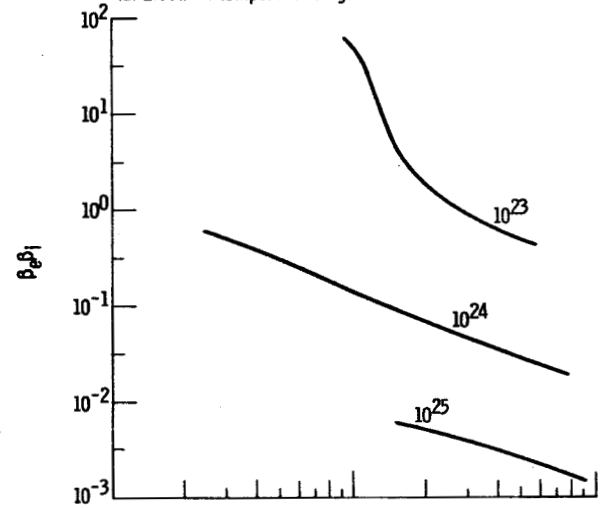

(b) $\beta_e\beta_i$ against effective electric field.

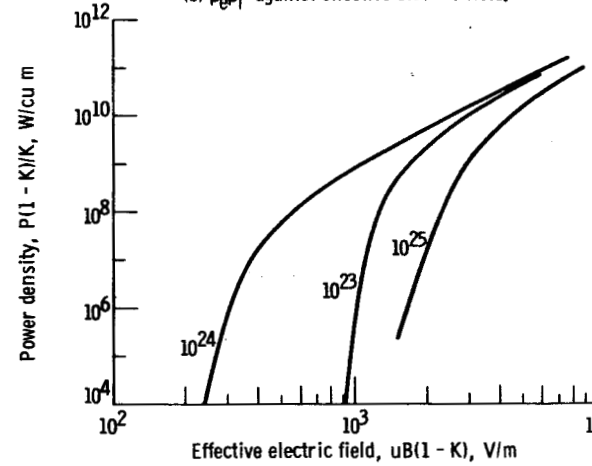

(c) Power density against effective electric field.

Figure 13. - Performance parameters as functions of electric field for unseeded neon. Magnetic field strength, 2 webers per square meter; static gas temperature, 500^0 K.

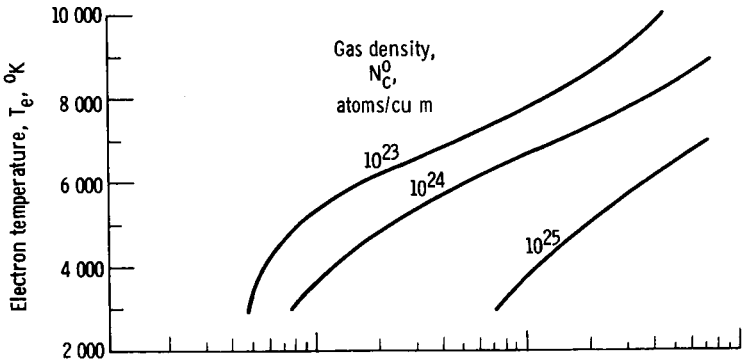

(a) Electron temperature against effective electric field.

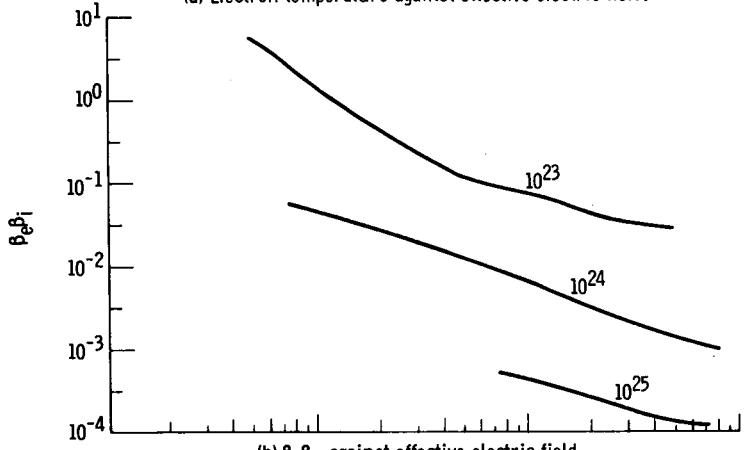

(b) $\beta_e\beta_i$ against effective electric field.

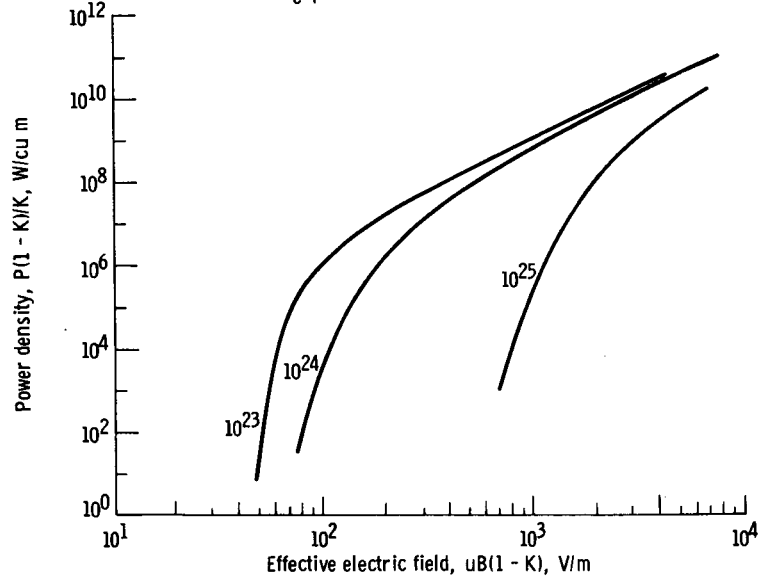

(c) Power density against effective electric field.

Figure 14. - Performance parameters as functions of electric field for unseeded xenon. Magnetic field strength, 2 webers per square meter; static gas temperature, 500° K.

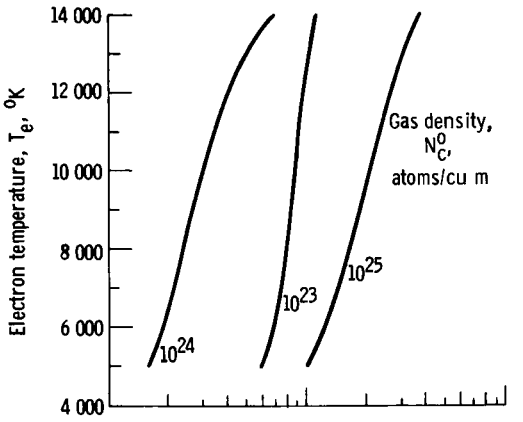

(a) Electron temperature against effective electric field.

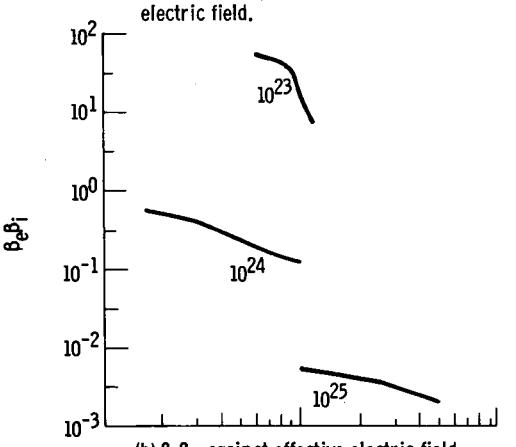

(b) $\beta_e\beta_i$ against effective electric field.

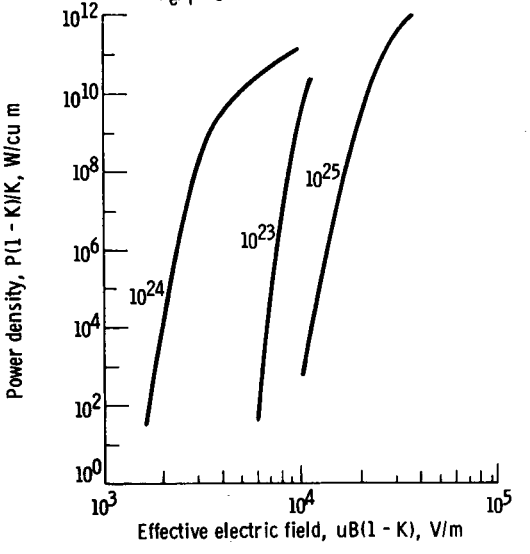

(c) Power density against effective electric field.

Figure 15. - Performance parameters as functions of electric field for unseeded helium. Magnetic field strength, 2 webers per square meter; static gas temperature, 500° K.

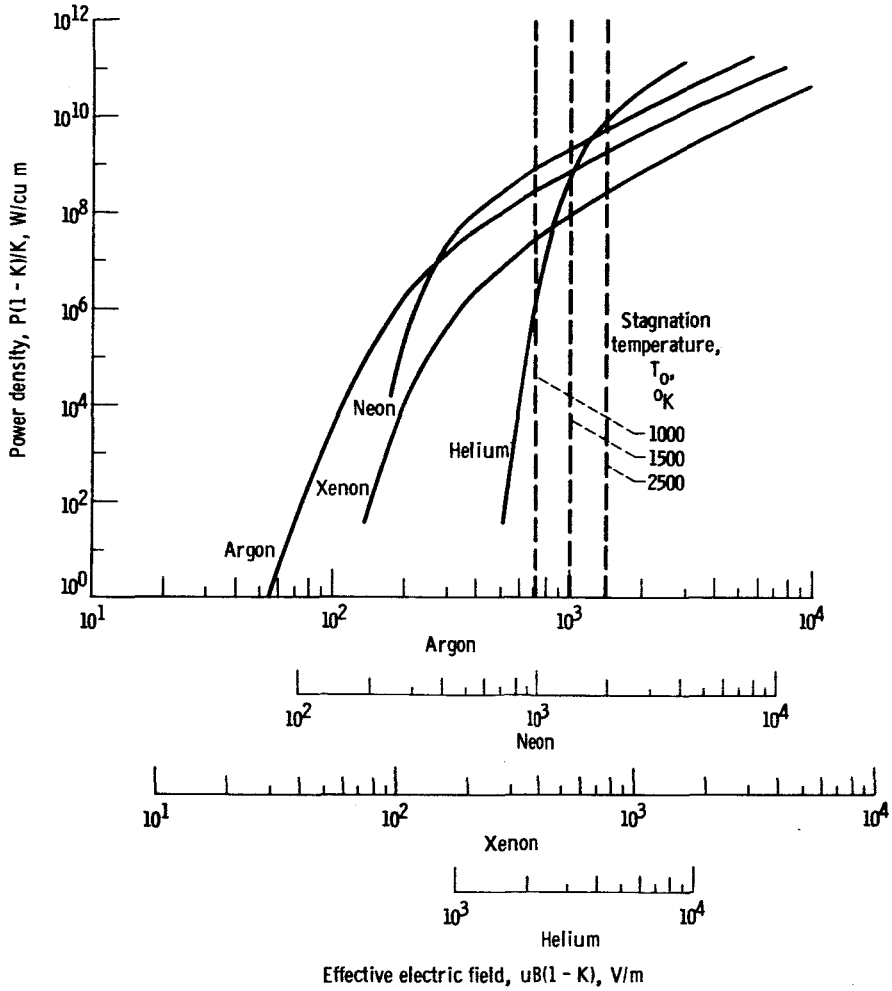

Figure 16. - Comparison of power densities of unseeded noble gases on basis of equal stagnation temperatures. Magnetic field strength, 2 webers per square meter; static gas temperature, 500° K; gas density, 10^{24} atoms per cubic meter.

quires the calculation of the power density for each combination at the operating conditions of interest and for various seed fractions. Since these calculations have been carried out in reference 5, including the variation in properties along the generator channel, extensive calculations of this nature are unwarranted for the purposes of this report. However, the magnitude of the power density for zero seed does provide an idea of the best choice of carrier gas. For assigned values of B, N_c^o, T_e, and T, uB(1 - K) is calculated from equation (24), and the result is substituted in equation (11) to yield the power density parameter P(1 - K)/K. The electron temperature T_e, $\beta_e\beta_i$, and P(1 - K)/K are plotted as a function of the effective electric field uB(1 - K) in figures 12 to 15 for unseeded argon, neon, xenon, and helium. Note that the scale of uB(1 - K) in the helium curves (fig. 15) extends one decade higher than the scales for the other gases. At any specified value of uB(1 - K), the power densities for argon equal or exceed those of the other gases. The single exception is xenon, which produces higher

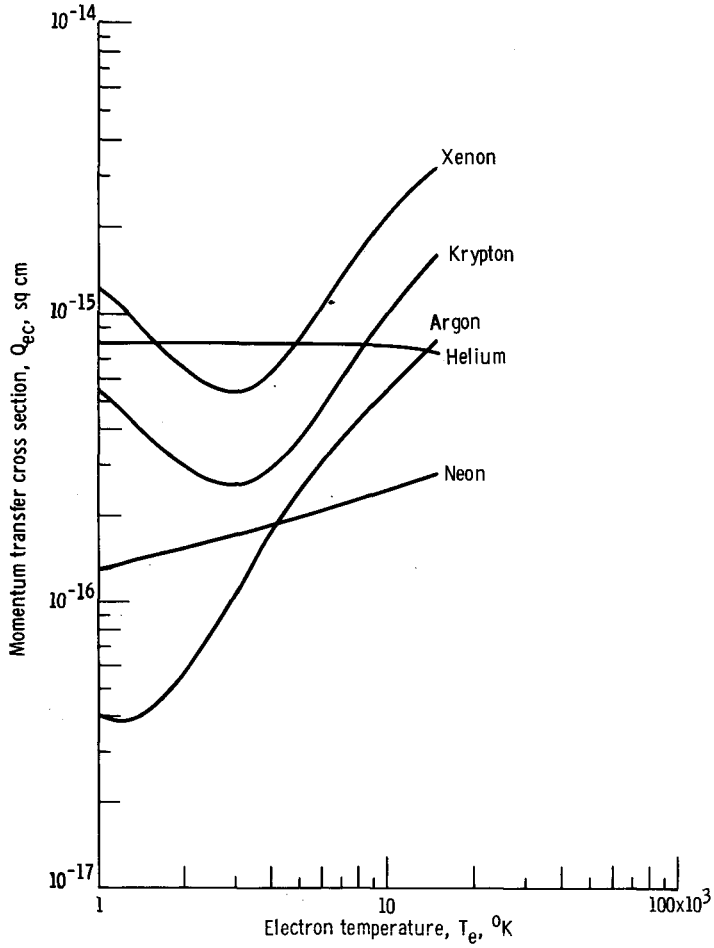

Figure 17. - Momentum transfer cross sections of noble gases.

power at a gas density of 10^{23} atoms per cubic meter because the mobility of xenon ions in xenon is smaller than that of argon ions in argon.

A comparison of power densities on the basis of equal stagnation temperatures, rather than equal values of uB(1 - K), is shown in figure 16. The curves shown are simply the curves of figures 12(c), 13(c), 14(c), and 15(c) for a gas density of 10^{24} atoms per cubic meter, a magnetic field of 2 webers per square meter, and a static gas temperature of 500^o K. The scales of uB(1 - K) are shifted so that a single vertical line corresponds to the same stagnation temperature for all four of the carrier gases. The dashed lines indicate a few stagnation temperatures. Any two of the abscissa scales are shifted with respect to each other by an amount equal to the square root of the ratio of their atomic weights, since $u = \sqrt{2c_p(T_0 - T)}$ and $c_p \propto 1/m_c$.

Figure 16 discloses that argon produces the highest power at low values of uB(1- K), but as uB(1 - K) increases, the power production in neon and helium exceeds that of argon. Although helium yields the highest power densities when uB(1 - K) is greater than about 4×10^3 volts per meter, argon and neon appear to be the best for operation over a wide range of uB(1 - K). The latter are in fact the carrier gases with the lowest electron elastic scattering cross sections at temperatures of the order of 1 electron volt. The complete channel calculations of Heighway and Nichols (ref. 5) showed that with regard to neon and argon carriers, the optimum overall power output for cesium-seeded argon was 15 percent larger than that for cesium-seeded neon. At the entrance section of their generator, however, neon-cesium yielded a power density about twice that for argon-cesium. The overall power output of cesium-seeded helium was found to be considerably less than that of argon and neon. These results can be understood on the basis of figure 16, since the power density in neon and helium, although larger at high values of uB(1 - K), fall off with decreasing uB(1 - K) faster than it does in argon.

In a supersonic, constant-area generator, uB(1 - K) drops off rapidly, as shown by the operating curve of figure 4(b), because u decreases and K increases, and therefore argon, which produces the highest power density at low values of uB(1 - K), also produces the highest overall power output. Although the gas density does not remain strictly constant through the generator, its variation is not significant, as can be seen from figure 4(b), and the interpretation of the results of reference 5 by means of the constant gas density curves of figure 16 should be qualitatively correct. The behavior of the curves of figure 16 is not surprising in view of the variation of the elastic-scattering cross sections of the noble gases (fig. 17, p. 26) with decreasing electron temperature.

The vertical lines in figure 16 corresponding to various stagnation temperatures were drawn under the assumption that $B(1 - K) = 1$ or $K = 0.5$ for the particular case shown of $B = 2$ webers per square meter.

CONCLUDING REMARKS

The consequences of the addition of alkali seed to a noble carrier gas in an MHD generator have been examined from the point of view of realizing magnetically induced nonequilibrium ionization. An examination of the physical bases of the results tends to identify the desirable properties of carrier and seed materials for this optimization of power density.

The important properties of carrier gases are that (1) they be of low molecular weight so as to yield large induced electric fields for a given stagnation temperature and (2) they have low cross sections to elastic scattering of electrons so that the electrons will tend to higher temperatures, resulting in high electric conductivity. The seed on the other hand should have (1) low ionization potential so that in low concentrations it is fully ionized, (2) high molecular weight to minimize electron energy loss, and (3) low cross sections to elastic scattering of electrons for the reason mentioned previously with regard to the carrier gas.

For the gas combinations considered herein, neon and argon appear to be the most suitable carrier gases while cesium is the most suitable seed. For reasonable generator operating conditions using these carriers, higher power densities will likely be obtained with seed rather than in the absence of seed and with cesium seed rather than with any lighter alkali gas.

It should be pointed out that the present analysis directly answers the question of whether the power density increases or decreases with the addition of seed only in the limiting case where the seed fraction approaches zero. The conclusions cannot be extended to arbitrary seed fractions since the power density does not necessarily vary monotonically with seed fraction. In fact, the results of reference 5 indicate that for a

case where the present analysis indicates the desirability of seeding there is an optimum seed fraction beyond which power density decreases with increase in seed fraction.

Another important restriction of the present analysis is due to the omission of inelastic collisions and radiation losses. The analysis of the combined effect of these processes on nonequilibrium ionization in a seeded plasma is a formidable problem, but one which is important enough to warrant further study.

Lewis Research Center,
National Aeronautics and Space Administration,
Cleveland, Ohio, January 12, 1965.

APPENDIX A

SYMBOLS

Mks units are used except where explicitly noted otherwise.

A	atomic weight
a	defined by eq. (29a)
B	magnetic field strength
b	defined by eq. (29b)
b_o	impact parameter for 90^o coulomb scattering
C_1, C_2, C_3, C_4	defined by eqs. (B15)
c	defined by eq. (29c)
D	defined by eq. (D22)
d	Debye length, eq. (C14)
E	electric field
e	electron charge, 1.602×10^{-19} C
g	ground state degeneracy
$g(T_e)$	defined by eq. (26)
h	Planck constant, 6.625×10^{-34} J-sec
J	current density
K	load parameter defined by eq. (6)
K_{rt}	defined by eq. (C3)
k	Boltzmann constant, 1.380×10^{-23} J/^{o}K
m_r	mass of particle of r^{th} species
m_{rt}	reduced mass of particles r and t
N_r	number of particles or r^{th} species per unit volume
N_r^o	sum of number densities of ions and atoms of species r
$(N_c^o)_{lim}$	defined by eq. (31)
N_0	standard gas density, 2.69×10^{19} atoms/cu cm
n	exponent in eq. (D11)
P	power density
Q_c	total cross section for scattering of monoenergetic beam, eq. (C25)
Q_m	momentum transfer cross section for scattering of monoenergetic beam defined by eq. (C6)
Q_{rt}	collision cross section for momentum transfer from species r to species t averaged over Maxwell distribution, eq. (C10)
R_{rt}	defined by eq. (D13)
s	seed fraction defined by eq. (12)
T	static gas temperature

T_r temperature of r^{th} species

u gas velocity

V_r ionization potential of r^{th} species

v relative speed of particles

v_r velocity of particle of r^{th} species

w_d difference in ion drift velocities defined by eq. (19)

w_i mean ion drift velocity defined by eq. (B8)

w_r drift velocity of r^{th} species

x_c degree of ionization of carrier gas defined by eq. (15)

x_s degree of ionization of seed defined by eq. (16)

$Z_{rt}^{(11)}$ cross section for momentum transfer from species r to species t averaged over Maxwell distribution defined by eq. (C5)

α mean thermal speed, eq. (C4)

β_e electron Hall parameter defined by eq. (9)

β_i ion slip parameter defined by eq. (10)

δ mean elastic energy loss factor defined by eq. (2)

ϵ defined by eq. (B31)

ϵ_o permittivity of free space, 8.854×10^{-12} F/m

Λ ratio of Debye radius to impact parameter for 90^o scattering defined by eq. (C16), eq. (C19)

λ defined by eq. (B20)

μ ion mobility

μ_0 ion mobility at 300^o K and gas density of 2.69×10^{19} atoms/cu cm

ν_e total electron collision frequency, eq. (8)

ν_{ia} effective ion-atom collision frequency defined by eq. (B19)

ν_{rt} mean collision frequency for momentum transfer from species r to species t

ρ gas density

σ_0 electrical conductivity

χ scattering angle in center of mass coordinates

Ψ defined by eq. (D18)

Ω scattering solid angle

ω_e electron cyclotron frequency

Subscripts:

a atom

c carrier gas atom

c^+ carrier gas ion

e electron

i ion

max maximum

min minimum

r	r^{th} species (r = e, i, a, c, c^+, s, s^+)	t	t^{th} species (t = e, i, a, c, c^+, s, s^+)
s	seed atom	0	stagnation conditions
s^+	seed ion	1	conditions at generator entrance

APPENDIX B

CALCULATION OF ION SLIP FOR TWO ION SPECIES

The drift motion of a species r of charged particles in crossed electric and magnetic fields is described by the momentum equation (ref. 4)

$$e_r(\vec{E}^* + \vec{w}_r \times \vec{B}) = \sum_t m_{rt}\nu_{rt}(\vec{w}_r - \vec{w}_t) \qquad (r = e,\ s^+,\ c^+;\ t = e,\ s^+,\ c^+,\ s,\ c) \qquad \text{(B1)}$$

where

$$\vec{E}^* \equiv \vec{E} + \vec{u} \times \vec{B} \qquad \text{(B2)}$$

is the effective electric field measured in a coordinate system moving with the mean gas velocity $\vec{u}$, and m_{rt} is the reduced mass of particles r and t, defined as

$$m_{rt} \equiv \frac{m_r m_t}{m_r + m_t} \qquad \text{(B3)}$$

When written out in full for the electrons e, carrier gas ions c^+, and seed ions s^+, equation (B1) becomes

$$\text{e:} \quad m_e\nu_{ec^+}\left(\vec{w}_e - \vec{w}_{c^+}\right) + m_e\nu_{es^+}\left(\vec{w}_e - \vec{w}_{s^+}\right) + m_e(\nu_{ec} + \nu_{es})\vec{w}_e = -e(\vec{E}^* + \vec{w}_e \times \vec{B}) \qquad \text{(B4)}$$

$$c^+\text{:} \quad m_e\nu_{c^+e}(\vec{w}_{c^+} - \vec{w}_e) + (m_{c^+c}\nu_{c^+c} + m_{c^+s}\nu_{c^+s})\vec{w}_{c^+} + m_{c^+s^+}\nu_{c^+s^+}\left(\vec{w}_{c^+} - \vec{w}_{s^+}\right) = e(\vec{E}^* + \vec{w}_{c^+} \times \vec{B}) \qquad \text{(B5)}$$

$$s^+\text{:} \quad m_e\nu_{s^+e}(\vec{w}_{s^+} - \vec{w}_e) + (m_{s^+c}\nu_{s^+c} + m_{s^+s}\nu_{s^+s})\vec{w}_{s^+} + m_{s^+c^+}\nu_{s^+c^+}\left(\vec{w}_{s^+} - \vec{w}_{c^+}\right) = e(\vec{E}^* + \vec{w}_{s^+} \times \vec{B}) \qquad \text{(B6)}$$

As in reference 4, the atom drift velocities are neglected, an assumption that is valid for small degrees of ionization.

In reference 4, the drift motion of a single ion species for an unseeded plasma in crossed electric and magnetic fields was described by the momentum equation

$$m_e \nu_{ie}(\vec{w}_i - \vec{w}_e) + \frac{m_c}{2}\nu_{ia}\vec{w}_i = e(\vec{E}^* + \vec{w}_i \times \vec{B}) \tag{B7}$$

The aim here is to derive a similar equation for the combined drift motion of the two ion species in the seeded plasma. To accomplish this, it is convenient to define a mean ion drift velocity as

$$\vec{w}_i \equiv \frac{N_{c+}\vec{w}_{c+} + N_{s+}\vec{w}_{s+}}{N_{c+} + N_{s+}} \tag{B8}$$

The difference in ion drift velocities

$$\vec{w}_d \equiv \vec{w}_{c+} - \vec{w}_{s+} \tag{B9}$$

is also a convenient quantity.

The following equation is obtained by multiplying equation (B5) by N_{c+}, equation (B6) by N_{s+}, adding and making use of the definitions of $\vec{w}_i$ and $\vec{w}_d$ (eqs. (B8) and (B9), respectively):

$$m_e\nu_{ie}(\vec{w}_i - \vec{w}_e) + \left[\frac{N_{c+}}{N_{c+} + N_{s+}}(m_{c+c}\nu_{c+c} + m_{c+s}\nu_{c+s}) + \frac{N_{s+}}{N_{c+} + N_{s+}}(m_{s+c}\nu_{s+c} + m_{s+s}\nu_{s+s})\right]\vec{w}_i + \frac{N_{c+}N_{s+}}{(N_{c+} + N_{s+})^2}\left[(m_{c+c}\nu_{c+c} + m_{c+s}\nu_{c+s}) - (m_{s+c}\nu_{s+c} + m_{s+s}\nu_{s+s})\right]\vec{w}_d = e(\vec{E}^* + \vec{w}_i \times \vec{B}) \tag{B10}$$

In reducing the first term of equation (B10) to this form, use was made of the fact that

$$\nu_{c+e} = \nu_{s+e} = \nu_{ie} \tag{B11}$$

since the ion-electron collision frequency involves only the electron number density and electron temperature and not the properties of the individual ions (provided all the ions are singly charged). Also, ion-ion collisions cancel out because of conservation of momentum in collisions.

An equation for the difference velocity $\vec{w}_d$ is formed by subtracting equation (B6) from equation (B5). The resulting equation becomes

$$\left[(m_{c+s+}\nu_{c+s+} + m_{s+c+}\nu_{s+c+} + m_e\nu_{ie}) + \frac{N_{c+}}{N_{c+} + N_{s+}}(m_{s+c}\nu_{s+c} + m_{s+s}\nu_{s+s})\right.$$

$$\left. + \frac{N_{s+}}{N_{c+} + N_{s+}}(m_{c+c}\nu_{c+c} + m_{c+s}\nu_{c+s})\right]\vec{w}_d - e\vec{w}_d \times \vec{B}$$

$$= -\left[(m_{c+c}\nu_{c+c} + m_{c+s}\nu_{c+s}) - (m_{s+c}\nu_{s+c} + m_{s+s}\nu_{s+s})\right]\vec{w}_i \qquad \text{(B12)}$$

If

$$m_{c+c}\nu_{c+c} + m_{c+s}\nu_{c+s} = m_{s+c}\nu_{s+c} + m_{s+s}\nu_{s+s} \qquad \text{(B13)}$$

then the ions drift with the same velocity. Since ν_{rt} is proportional to N_t, equation (B13) can be satisfied for arbitrary seed and carrier gas densities only if the collision coefficients for each ion species with the seed and carrier gas atoms are the same, that is, only if

$$m_{c+c}\nu_{c+c} = m_{s+c}\nu_{s+c} \qquad \text{(B14a)}$$

$$m_{c+s}\nu_{c+s} = m_{s+s}\nu_{s+s} \qquad \text{(B14b)}$$

Unfortunately, conditions (B14) are generally not satisfied. Therefore, it is necessary to solve equation (B12) for $\vec{w}_d$ in terms of $\vec{w}_i$ and substitute the result in equation (B10). The following abbreviations are introduced:

$$C_1 \equiv m_{c+c}\nu_{c+c} + m_{c+s}\nu_{c+s} \qquad \text{(B15a)}$$

$$C_2 \equiv m_{s+c}\nu_{s+c} + m_{s+s}\nu_{s+s} \qquad \text{(B15b)}$$

$$C_3 \equiv m_{c+s+}\nu_{c+s+} + m_{s+c+}\nu_{s+c+} + m_e\nu_{ie} \tag{B15c}$$

$$C_4 \equiv C_3 + \frac{N_{c+}C_2 + N_{s+}C_1}{N_{c+} + N_{s+}} \tag{B15d}$$

When compared to the other terms in equation (B15c), $m_e\nu_{ie}$ is of the order (m_e/m_i) and therefore may be neglected. Then equation (B12) may be rewritten as

$$\left(1 + \frac{e\vec{B}}{C_4}\times\right)\vec{w}_d = -\frac{C_1 - C_2}{C_4}\vec{w}_i \tag{B16}$$

which may be easily solved by premultiplying both sides by the operator

$$1 - \frac{e\vec{B}}{C_4}\times$$

and using the fact that $\vec{w}_d$ is perpendicular to $\vec{B}$. Then

$$\vec{w}_d = -\frac{C_1 - C_2}{C_4}\frac{1}{1 + \left(\frac{eB}{C_4}\right)^2}\left(\vec{w}_i + \frac{e}{C_4}\vec{w}_i \times \vec{B}\right) \tag{B17}$$

If equation (B17) is substituted into equation (B10), the resulting equation can be written in a form quite similar to that of equation (B7), namely,

$$m_e\nu_{ie}(\vec{w}_i - \vec{w}_e) + \frac{m_c}{2}\nu_{ia}\vec{w}_i = e\left[\vec{E}^* + (1 + \lambda)\vec{w}_i \times \vec{B}\right] \tag{B18}$$

where now the effective ion-neutral collision frequency is defined as

$$\nu_{ia} \equiv \frac{2}{m_c}\left[\frac{x_c}{x_c + sx_s}C_1 + \frac{sx_s}{x_c + sx_s}C_2 - \frac{sx_sx_c}{(x_c + sx_s)^2}\frac{(C_1 - C_2)^2}{C_4}\frac{1}{1 + \left(\frac{eB}{C_4}\right)^2}\right] \tag{B19}$$

and

$$\lambda \equiv \frac{sx_s x_c}{(x_c + sx_s)^2} \frac{(C_1 - C_2)^2}{C_4^2} \frac{1}{1 + \left(\frac{eB}{C_4}\right)^2} \tag{B20}$$

The collision frequency for electrons with any single ion species A^+ in a mixture of singly charged ions is

$$\nu_{eA^+} = N_{A^+} Q_{ei} \langle v_e \rangle \tag{B21}$$

where the electron-ion collision cross section Q_{ei} is determined by the coulomb interaction between electron and ion and is therefore the same for all singly charged ions (see appendix C for the exact expression). In the present case, the total electron-ion collision frequency is

$$\nu_{ei} = \nu_{ec^+} + \nu_{es^+} = N_i Q_{ei} \langle v_e \rangle \tag{B22}$$

where

$$N_i = N_{c^+} + N_{s^+} \tag{B23}$$

If the total electron-atom collision frequency is written

$$\nu_{ea} = \nu_{ec} + \nu_{es} \tag{B24}$$

and use is made of the definition of $\vec{w}_i$ (eq. (B8)) and equations (B22) and (B23), equation (B4) may be written in the form

$$m_e \nu_{ei} (\vec{w}_e - \vec{w}_i) + m_e \nu_{ea} \vec{w}_e = -e(\vec{E}^* + \vec{w}_e \times \vec{B}) \tag{B25}$$

which is identical to equation (36) of reference 4.

Ohm's law and the expression for the electron heating rate are obtained from equations (B18) and (B25). The total current

$$\vec{J} = N_e e(\vec{w}_i - \vec{w}_e) \tag{B26}$$

and the electron current

$$\vec{J}_e = - N_e e \vec{w}_e \tag{B27}$$

are introduced into equations (B25) and (B18), which become

$$-m_e \nu_{ei} \vec{J} - m_e \nu_{ea} \vec{J}_e = -N_e e^2 \vec{E}^* + e \vec{J}_e \times \vec{B} \tag{B28}$$

$$m_e \nu_{ei} \vec{J} + \frac{m_c}{2} \nu_{ia} (\vec{J} - \vec{J}_e) = N_e e^2 \vec{E}^* + e(1 + \lambda)(\vec{J} - \vec{J}_e) \times \vec{B} \tag{B29}$$

Addition of equations (B28) and (B29) and solution of the resulting equation for $\vec{J}_e$ by the same device as employed in the solution of equation (B16) yield

$$\vec{J}_e = \frac{1}{(1 + \epsilon)^2 + \lambda^2 \beta_i^2} \left\{ \left[1 + \epsilon + \lambda(1 + \lambda)\beta_i^2 \right] \vec{J} + \beta_i \left[1 + \epsilon(1 + \lambda) \right] \frac{\vec{B}}{B} \times \vec{J} \right\} \tag{B30}$$

where

$$\epsilon \equiv 2 \frac{m_e}{m_c} \frac{\nu_{ea}}{\nu_{ia}} \tag{B31}$$

and

$$\beta_i \equiv \frac{2eB}{m_c \nu_{ia}} \tag{10}$$

Equation (B30) is substituted into equation (B28), which may then be put in the following form:

$$\sigma_0 \vec{E}^* = \frac{1}{(1 + \epsilon)^2 + \lambda^2 \beta_i^2} \left(\left\{ \frac{\nu_{ei}}{\nu_e} \left[(1 + \epsilon)^2 + \lambda^2 \beta_i^2 \right] + \frac{\nu_{ea}}{\nu_e} \left[1 + \epsilon + \lambda(1 + \lambda)\beta_i^2 \right] \right.\right.$$

$$\left.\left. + \beta_e \beta_i \left[1 + \epsilon(1 + \lambda) \right] \right\} \vec{J} - \beta_e \left\{ 1 + \epsilon + \lambda(1 + \lambda)\beta_i^2 - \epsilon \left[1 + \epsilon(1 + \lambda) \right] \right\} \frac{\vec{B}}{B} \times \vec{J} \right) \tag{B32}$$

where σ_0 is the conductivity

$$\sigma_0 = \frac{N_e e^2}{m_e \nu_e} \tag{7}$$

and the electron Hall parameter β_e is defined as

$$\beta_e \equiv \frac{\omega_e}{\nu_e} \equiv \frac{eB}{m_e \nu_e} \tag{9}$$

The electron heating rate $\vec{J}_e \cdot \vec{E}^*$ is, from equations (B30) and (B32)

$$\vec{J}_e \cdot \vec{E}^* = \frac{J^2}{\sigma_0} \frac{1}{\left[(1+\epsilon)^2 + \lambda^2\beta_i^2\right]^2} \left(\left[1 + \epsilon + \lambda(1+\lambda)\beta_i^2\right] \left\{ \frac{\nu_{ei}}{\nu_e} \left[(1+\epsilon)^2 + \lambda^2\beta_i^2\right] + \frac{\nu_{ea}}{\nu_e} \left[1 + \epsilon + \lambda(1+\lambda)\beta_i^2\right] \right\} + \beta_e\beta_i\epsilon \left[1 + \epsilon(1+\lambda)\right]^2 \right) \tag{B33}$$

Since ϵ and β_i^2 are both much smaller than 1, and λ for small seed fractions ($s < 0.1$) is of order 1 or less, terms of order ϵ, $\epsilon\lambda$, and $\lambda^2\beta_i^2$ can be neglected in equations (B32) and (B33). Thus, the simplified equations are

$$\sigma_0 \vec{E}^* = (1 + \beta_e\beta_i)\vec{J} - \beta_e \frac{\vec{B}}{B} \times \vec{J} \tag{B34}$$

$$\vec{J}_e \cdot \vec{E}^* = \frac{J^2}{\sigma_0} \tag{B35}$$

which are formally identical to equations (49) and (51) of reference 4. The only modification is that ν_{ia} is defined differently now (eq. (B19)). In the limit of zero seed, ν_{ia} reduces to ν_{c+c}, as it should.

APPENDIX C

MOMENTUM TRANSFER CROSS SECTIONS AND COLLISION FREQUENCIES

The collision frequencies ν_{rt} used in this report refer to the average rate of momentum transfer from species r to species t per particle of species r. The average rate of momentum transfer from species r is

$$\int m_r \vec{v}_r \left(\frac{\delta f_r}{\delta t}\right)_{coll} d^3 v_r \tag{C1}$$

where $(\delta f_r/\delta t)_{coll}$ denotes the rate of change of the distribution function f_r due to collisions. Burgers (refs. 6 and 7) has obtained an explicit expression for (C1) by assuming that the distribution function is close to Maxwellian. In the first approximation, he obtains

$$\int m_r \vec{v}_r \left(\frac{\delta f_r}{\delta t}\right)_{coll} d^3 v_r = - \sum_t K_{rt}(\vec{w}_r - \vec{w}_t) \tag{C2}$$

where $\vec{w}_r$ and $\vec{w}_t$ are the drift velocities. The friction coefficient K_{rt} is defined as

$$K_{rt} \equiv \frac{2}{3} m_{rt} N_r N_t \alpha Z_{rt}^{(11)} \tag{C3}$$

where m_{rt} is the reduced mass

$$m_{rt} \equiv \frac{m_r m_t}{m_r + m_t} \tag{B3}$$

α is a mean thermal speed[2]

---

[2]As noted in reference 4, Burgers' results apply to only the case $T_r = T_t = T$, but equation (C4) represents the proper generalization of Burgers' work to the case of different temperatures.

$$\alpha = \left(\frac{2kT_r}{m_r} + \frac{2kT_t}{m_t}\right)^{1/2} \tag{C4}$$

and $Z_{rt}^{(11)}$ is an averaged cross section for momentum transfer, defined as

$$Z_{rt}^{(11)} \equiv \frac{4}{\pi^{1/2}\alpha^6}\int_0^\infty v^5 Q_m(v)\exp\left(-\frac{v^2}{\alpha^2}\right)dv \tag{C5}$$

where $v = |\vec{v}_r - \vec{v}_t|$ is the relative speed.

The quantity Q_m (which Burgers denotes $S_{rt}^{(1)}$) appearing in the integrand is the momentum transfer collision cross section for a beam of particles of velocity v and is defined as

$$Q_m(v) \equiv \int \sigma(v,\chi)(1 - \cos\chi)d\Omega \tag{C6}$$

where $\sigma(v,\chi)$ is the differential cross section for scattering through the angle χ and $d\Omega$ the element of solid angle.

The relation between ν_{rt} and K_{rt} is (refs. 4 and 8)

$$\nu_{rt} = \frac{K_{rt}}{m_{rt}N_r} = \frac{2}{3}\alpha N_t Z_{rt}^{(11)} \tag{C7}$$

More often, the 2/3 factor is absorbed into the cross section, and the average value of the relative speed, which is

$$\langle v\rangle = \left(\frac{8kT_r}{\pi m_r} + \frac{8kT_t}{\pi m_t}\right)^{1/2} \tag{C8}$$

is used in place of α. Then ν_{rt} is written in the conventional definition as

$$\nu_{rt} = N_t\langle v\rangle Q_{rt} \tag{C9}$$

Clearly,

$$Q_{rt} = \frac{\sqrt{\pi}}{3} Z_{rt}^{(11)} \tag{C10}$$

For collisions between electrons and atoms or ions, the relative speed v is very nearly equal to v_e, and $\alpha \approx (2kT_e/m_e)^{1/2}$; hence equations (C10) and (C5) may be reduced to

$$Q_{et}(T_e) = \frac{4}{3}\left(\frac{m_e}{2kT_e}\right)^3 \int_0^\infty v_e^5 Q_m(v_e) \exp\left(-\frac{m_e v_e^2}{2kT_e}\right) dv_e \qquad (t = i, a) \tag{C11}$$

The well-known Rutherford cross section

$$\sigma(v_e, \chi) = \frac{1}{4}\left(\frac{e^2}{4\pi\epsilon_o}\right)^2 \frac{1}{m_e^2 v_e^4} \frac{1}{\sin^4 \frac{\chi}{2}} \tag{C12}$$

is used to calculate Q_m for collisions of electrons with singly charged ions. When equation (C12) and the formula $d\Omega = 2\pi \sin \chi \, d\chi$ are substituted into equation (C6) and the integration is performed over all scattering angles from 0 to π, the result is

$$Q_m = 4\pi\left(\frac{e^2}{4\pi\epsilon_o}\right)^2 \frac{1}{m_e^2 v_e^4} \left[\ln \sin \frac{\chi}{2}\right]_0^\pi \tag{C13}$$

Due to the long range nature of the coulomb potential, this integral diverges at the lower limit. Actually, the maximum range of the electrostatic field of an ion is of the order of the Debye length, which is (ref. 9)

$$d = \left(\frac{\epsilon_o kT_e}{N_e e^2}\right)^{1/2} \tag{C14}$$

At distances larger than d, electrons almost completely screen the field of the ion. Hence it is customary to replace the lower limit in equation (C13) by the minimum scattering angle χ_{min}, which is determined from the relation

$$\tan \frac{\chi_{min}}{2} = \frac{1}{\Lambda} \tag{C15}$$

where Λ is the ratio of the Debye length to the impact parameter b_o for 90^o scattering (ref. 9)

$$\Lambda \equiv \frac{d}{b_o} = \frac{\left(\frac{\epsilon_o kT_e}{N_e e^2}\right)^{1/2}}{\frac{e^2}{4\pi\epsilon_o}\frac{1}{m_e v_e^2}} \tag{C16}$$

Ions also contribute to the screening effect, but as pointed out in reference 10, the time involved in an encounter between an electron and an ion is much smaller than the period of oscillation of the ions; hence, there is not enough time for the ions to respond to the fluctuation in charge caused by the passing electron, and the ions therefore cannot provide effective screening for electron-ion collisions.

The result of cutting off the integral in Q_m at χ_{min} is therefore

$$Q_m = 2\pi \left(\frac{e^2}{4\pi\epsilon_o}\right)^2 \frac{1}{m_e^2 v_e^4} \ln(\Lambda^2 + 1) \tag{C17}$$

or since $\Lambda^2 >> 1$

$$Q_m \approx 4\pi \left(\frac{e^2}{4\pi\epsilon_o}\right)^2 \frac{1}{m_e^2 v_e^4} \ln \Lambda \tag{C18}$$

On account of the slow variation of $\ln \Lambda$ with v_e, it is also customary to replace $m_e v_e^2$ in equation (C16) by its average value, $3kT_e$, so that Λ becomes

$$\Lambda = \frac{12\pi(\epsilon_o kT_e)^{3/2}}{e^3 N_e^{1/2}} \tag{C19}$$

Integration of the expression (C18) according to equation (C11) yields finally the average momentum transfer cross section for electron-ion collisions

$$Q_{ei} = \frac{2\pi}{3}\left(\frac{e^2}{4\pi\epsilon_o}\right)^2 \frac{\ln \Lambda}{(kT_e)^2} \tag{C20}$$

The ion-ion cross section for singly charged ions is derived from equations (C5) and (C10) by using a Rutherford cross section similar to equation (C12), but with m_e replaced by the reduced mass of the ions and v_e by the relative speed v of the ions. The screening due to ions must also be included, since the ion-ion collision time is of the same order as the ion oscillation period. The correct Debye length d', including the effect of ion screening, is (ref. 10)

$$\frac{1}{d'^2} = \frac{1}{d^2} + \frac{1}{d_i^2} \tag{C21}$$

where

$$d_i = \left(\frac{\epsilon_o kT_i}{N_i e^2}\right)^{1/2} \tag{C22}$$

The result for the ion-ion cross section is

$$Q_{ii} = \frac{\pi}{3}\left(\frac{e^2}{4\pi\epsilon_o}\right)^2 \frac{\ln(\Lambda'^2 + 1)}{(kT_i)^2} \tag{C23}$$

where Λ' is the ratio of the Debye length d' to the average impact parameter for 90^o scattering of ions $(e^2/4\pi\epsilon_o)/3kT_i$

$$\Lambda' = \frac{12\pi(\epsilon_o kT_i)^{3/2}}{e^3 N_i^{1/2}} \left(1 + \frac{T_i}{T_e}\right)^{-1/2} \tag{C24}$$

The ion temperature is assumed to be equal to the gas temperature T. Since

$T_e >> T$, the last factor in equation (C24) may be set equal to one. However, $\Lambda' << \Lambda$, and it is generally incorrect to make the approximation $\Lambda' >> 1$ in equation (C23).

For electron-atom collisions, experimental values of the momentum transfer cross section Q_m were used. The authors of reference 5 have evaluated $Q_{et}(T_e)$ numerically for a number of gases in the range of T_e from 100° to $15\,000^\circ$ K. Where experimental values of Q_m were not available, they used the total cross section

$$Q_c(v_e) = \int \sigma(v_e, \chi) d\Omega \tag{C25}$$

instead. The difference between Q_m and Q_c for most gases is less than 10 percent (ref. 11, p. 31). The results for $Q_{ec}(T_e)$ for the noble gases are summarized in figure 17 on page 26.

In reference 4, it was assumed that electron-atom collisions could be treated by the hard-sphere model, in which Q_m is independent of v_e. In that case, equation (C11) yields

$$Q_{ec} = \frac{4}{3} Q_m \tag{C26}$$

A constant value of $Q_m = 2.0 \times 10^{-17}$ square centimeter was used for argon in references 1, 3, and 4. This value was inferred from monoenergetic cross section data (ref. 11, p. 19), which showed little variation over a range of electron energies below 1 electron volt. From figure 17 it can be seen that this value was far too low. The average momentum transfer cross section also rises rather rapidly with electron temperature. The necessity of using the properly averaged cross section is apparent.

The momentum transfer frequencies for ion-atom collisions are calculated from ionic mobility data. The mobility μ_{rt} of an ion of species r in a gas of species t is defined as

$$\vec{w}_r = \mu_{rt} \vec{E} \tag{C27}$$

where $\vec{w}_r$ is the drift velocity and $\vec{E}$ is the electric field. Comparison of equations (B1) and (C27) shows that the mobility for singly charged ions is related to the average momentum transfer ν_{rt} by the formula

$$\mu_{rt} = \frac{e}{m_{rt} \nu_{rt}} \tag{C28}$$

Note that ν_{rt} is proportional and μ_{rt} is inversely proportional to the density N_t. Experimental mobilities are often referred to the standard gas density $N_0 = 2.69 \times 10^{19}$ atoms per cubic centimeter and the corresponding mobility denoted by μ_0, as in reference 11, so that the mobility μ at any other gas density N is

$$\mu = \mu_0 \frac{N_0}{N} \tag{C29}$$

APPENDIX D

DERIVATION OF BREAK-EVEN CONDITION

The derivatives dN_e/ds, $d\nu_e/ds$, $d\nu_{ia}/ds$, and $d\delta/ds$ are required for the evaluation of dT_e/ds and dP/ds from equations (20) and (22). Since the former quantities are functions of the degrees of ionization x_c and x_s of the carrier and seed gases, it is convenient to first calculate dx_c/ds and dx_s/ds.

Differentiation of equations (18) and (19) with respect to s and solution of the resulting equations for dx_c/ds and dx_s/ds yield

$$\frac{dx_c}{ds} = \frac{x_c(1 - x_c)}{x_c(1 - x_c) + sx_s(1 - x_s) + x_c + sx_s}\left\{\left[(x_c + sx_s)\left(\frac{3}{2} + \frac{eV_c}{kT_e}\right) + sx_s(1 - x_s)\,\frac{e(V_c - V_s)}{kT_e}\right]\frac{1}{T_e}\frac{dT_e}{ds} - x_s\right\} \tag{D1}$$

$$\frac{dx_s}{ds} = \frac{x_s(1 - x_s)}{x_c(1 - x_c) + sx_s(1 - x_s) + x_c + sx_s}\left\{\left[(x_c + sx_s)\left(\frac{3}{2} + \frac{eV_s}{kT_e}\right) - x_c(1 - x_c)\,\frac{e(V_c - V_s)}{kT_e}\right]\frac{1}{T_e}\frac{dT_e}{ds} - x_s\right\} \tag{D2}$$

Only the limiting forms of these expressions for $s = 0$ will be used here. It will be assumed that, in the limit of zero seed, the degree of ionization x_s of the seed approaches unity. Numerical calculations carried out in the course of the work reported in reference 4 for $s \leq 0.01$ support this assumption over the range of electron temperatures of interest. In fact, if s is set equal to zero in equations (18) and (19) for $x_c \ll 1$, the following expressions are obtained for x_c and x_s:

$$x_c = \sqrt{F_c} \tag{D3a}$$

$$x_s \approx \frac{1}{1 + \dfrac{\sqrt{F_c}}{F_s}} \tag{D3b}$$

where F_s amd F_c are the right sides of equations (18) and (19), respectively. The ionization potential of the carrier gas is several times larger than that of the seed, so that $F_c \ll F_s$; and since $F_s > 1$ for the range of electron temperatures of interest here, $x_s = 1$ to a high degree of approximation.

With the aforementioned assumptions, in the limit of zero seed, equation (D1) reduces to

$$\left(\frac{dx_c}{ds}\right)_{s=0} = \frac{1 - x_c}{2 - x_c}\left[x_c\left(\frac{3}{2} + \frac{eV_c}{kT_e}\right)\frac{1}{T_e}\left(\frac{dT_e}{ds}\right)_{s=0} - 1\right] \tag{D4}$$

Since dx_s/ds appears everywhere multiplied by s, its limiting expression for $s = 0$ is not required.

From equation (17), for $x_s = 1$,

$$\frac{1}{N_e}\left(\frac{dN_e}{ds}\right)_{s=0} = \frac{1}{x_c}\left[\left(\frac{dx_c}{ds}\right)_{s=0} + 1\right] = \frac{1 - x_c}{2 - x_c}\left[\left(\frac{3}{2} + \frac{eV_c}{kT_e}\right)\frac{1}{T_e}\left(\frac{dT_e}{ds}\right)_{s=0} + \frac{1}{x_c(1 - x_c)}\right] \tag{D5}$$

Substitution of equation (D5) into equation (20) yields the expression

$$\frac{1}{P}\left(\frac{dP}{ds}\right)_{s=0} = \frac{1}{2}\left\{\left[\frac{2(1 - x_c)}{2 - x_c}\left(\frac{3}{2} + \frac{eV_c}{kT_e}\right) + \frac{T_e}{T_e - T}\right]\frac{1}{T_e}\left(\frac{dT_e}{ds}\right)_{s=0} + \frac{2}{x_c(2 - x_c)} + \frac{1}{\delta}\left(\frac{d\delta}{ds}\right)_{s=0}\right\} \tag{D6}$$

The various derivatives in equation (22) will now be calculated. The total electron collision frequency is written

$$\nu_e = \nu_{ec} + \nu_{es} + \nu_{ei} \tag{D7}$$

where

$$\nu_{ec} = N_c Q_{ec}\langle v_e\rangle = N_c^o(1 - x_c)Q_{ec}\langle v_e\rangle \tag{D8}$$

$$\nu_{es} = N_s Q_{es}\langle v_e\rangle = N_c^o s(1 - x_s)Q_{es}\langle v_e\rangle \tag{D9}$$

$$\nu_{ei} = \nu_{ec^+} + \nu_{es^+} = N_i Q_{ei} \langle v_e \rangle = N_c^o (x_c + s x_s) Q_{ei} \langle v_e \rangle \tag{D10}$$

The electron-ion cross section Q_{ei} is proportional to T_e^{-2}, as can be seen from equation (C20). For the electron-atom cross sections the variation with electron temperature is expressed by relations of the form

$$Q_{ec} = (\text{const}) T_e^n \tag{D11}$$

in the immediate vicinity of the electron temperature corresponding to zero seed. The exponent n is taken from the slope of a log-log plot of Q_{ec} as a function of T_e. The method of deducing the average momentum transfer cross section $Q_{ec}(T_e)$ from experimental data on the momentum transfer cross section $Q_m(v_e)$ for a monoenergetic beam of electrons is described in appendix C.

The derivative of ν_e with respect to s can be calculated in a straightforward manner using equations (D7) to (D11) and (D4). The slight variation of ln Λ with s can be neglected. In the limit of zero seed the result becomes

$$\frac{1}{\nu_e}\left(\frac{d\nu_e}{ds}\right)_{s=0} = \frac{1}{2}\left\{\frac{\nu_{ec}}{\nu_e}\left[2n + 1 - \frac{2x_c}{2 - x_c}\left(\frac{3}{2} + \frac{eV_c}{kT_e}\right)\right] + \frac{\nu_{ei}}{\nu_e}\left[-3 + \frac{2(1 - x_c)}{2 - x_c}\left(\frac{3}{2} + \frac{eV_c}{kT_e}\right)\right]\right\}\frac{1}{T_e}\left(\frac{dT_e}{ds}\right)_{s=0} + \frac{1}{2 - x_c}\left(\frac{\nu_{ec}}{\nu_e} + \frac{1}{x_c}\frac{\nu_{ei}}{\nu_e}\right) \tag{D12}$$

The calculation of $d\nu_{ia}/ds$ is also straightforward. It is convenient to use the abbreviation

$$R_{rt} \equiv \frac{m_{rt}\nu_{rt}}{N_t} = R_{tr} \tag{D13}$$

where ion-ion and ion-atom collisions are involved, since this quantity is independent of s. Then the quantities C_1, C_2, and C_3, which enter into the expression (B19) for ν_{ia} become

$$C_1 = \left[(1 - x_c)R_{c^+c} + s(1 - x_s)R_{c^+s}\right]N_c^o \tag{D14}$$

$$C_2 = \left[(1 - x_c)R_{s+c} + s(1 - x_s)R_{s+s}\right]N_c^o \tag{D15}$$

$$C_3 = (x_c + sx_s)R_{s+c+}N_c^o \tag{D16}$$

Substitution of equations (D14) to (D16) into equation (B19) and differentiation of the result with respect to s yields in the limit of zero seed

$$\frac{1}{\nu_{ia}}\left(\frac{d\nu_{ia}}{ds}\right)_{s=0} = -\frac{1}{1 - x_c}\left(\frac{dx_c}{ds}\right)_{s=0} + \frac{1}{x_c}\Psi = -\frac{x_c}{2 - x_c}\left(\frac{3}{2} + \frac{eV_c}{kT_e}\right)\frac{1}{T_e}\left(\frac{dT_e}{ds}\right)_{s=0} + \frac{1}{2 - x_c} + \frac{1}{x_c}\Psi \tag{D17}$$

where the expression (D4) has been used for $(dx_c/ds)_{s=0}$, and the following notation has been introduced for brevity:

$$\Psi \equiv \left(\frac{R_{s+c}}{R_{c+c}} - 1\right)\frac{(1 - x_c)R_{c+c} + x_cR_{s+c+}}{(1 - x_c)R_{s+c} + x_cR_{s+c+}} \tag{D18}$$

In obtaining equations (D17) and (D18), use was made of the approximation $(eB/C_4)^2 << 1$. This approximation is consistent with the assumptions of appendix B since the quantity $(eB/C_4)^2$ is of the same order as β_i^2.

Finally, the derivative $d\delta/ds$ is calculated from the expression

$$\delta = \frac{1}{\nu_e}\left[\nu_{ec} + \nu_{ec+} + \frac{m_c}{m_s}(\nu_{es} + \nu_{es+})\right] = 1 + \left(\frac{m_c}{m_s} - 1\right)\frac{\nu_{es} + \nu_{es+}}{\nu_e} \tag{D19}$$

and the result in the limit $s = 0$ is

$$\frac{1}{\delta}\left(\frac{d\delta}{ds}\right)_{s=0} = \frac{1}{x_c}\left(\frac{m_c}{m_s} - 1\right)\frac{\nu_{ei}}{\nu_e} \tag{D20}$$

Substitution of equations (D12), (D17), and (D20) into equation (22) yields the following equation for $(dT_e/ds)_{s=0}$:

$$\frac{1}{Te}\left(\frac{dT_e}{ds}\right)_{s=0} = -\frac{1}{x_c D}\left\{\frac{2x_c}{2-x_c}\frac{\nu_{ec}}{\nu_e} + \left[\frac{2}{2-x_c} - \left(1 - \frac{m_c}{m_s}\right)\right]\frac{\nu_{ei}}{\nu_e} - \beta_e\beta_i\left[\left(1 - \frac{m_c}{m_s}\right)\frac{\nu_{ei}}{\nu_e} + \frac{2x_c}{2-x_c} + 2\Psi\right]\right\} \quad \text{(D21)}$$

where

$$D \equiv \frac{\nu_{ec}}{\nu_e}\left[2n + 1 + \frac{T_e}{T_e - T} - \frac{2x_c}{2-x_c}\left(\frac{3}{2} + \frac{eV_c}{kT_e}\right)\right] + \frac{\nu_{ei}}{\nu_e}\left[-3 + \frac{T_e}{T_e - T} + \frac{2(1-x_c)}{2-x_c}\left(\frac{3}{2} + \frac{eV_c}{kT_e}\right)\right] + \beta_e\beta_i\left[\frac{T_e}{T_e - T} + \frac{2x_c}{2-x_c}\left(\frac{3}{2} + \frac{eV_c}{kT_e}\right)\right] \quad \text{(D22)}$$

Substituting equation (D21) into equation (D6) and rearranging yields the result

$$\frac{1}{P}\left(\frac{dP}{ds}\right)_{s=0} = \frac{1}{x_c(2-x_c)}\frac{N}{D} \quad \text{(D23)}$$

where the numerator N is defined as

$$N \equiv \frac{\nu_{ec}}{\nu_e}\left[2n + 1 + \frac{T_e}{T_e - T} - x_c\left(3 - \frac{2eV_c}{kT_e} + \frac{T_e}{T_e - T}\right)\right] - 3\frac{\nu_{ei}}{\nu_e} + \beta_e\beta_i\left\{\frac{T_e}{T_e - T} + \Psi\left[(1-x_c)\left(3 + \frac{2eV_c}{kT_e} + \frac{T_e}{T_e - T}\right) + \frac{T_e}{T_e - T}\right] + x_c\left(3 + \frac{2eV_c}{kT_e} + \frac{T_e}{T_e - T}\right)\right\} - \left(1 - \frac{m_c}{m_s}\right)\frac{\nu_{ei}}{\nu_e}\left\{\frac{\nu_{ec}}{\nu_e}\left[\left(1 - \frac{x_c}{2}\right)(2n+1) - \left(\frac{3}{2} + \frac{eV_c}{kT_e}\right)\right] - 3\left(1 - \frac{x_c}{2}\right)\frac{\nu_{ei}}{\nu_e} - \beta_e\beta_i(1-2x_c)\left(\frac{3}{2} + \frac{eV_c}{kT_e}\right)\right\} \quad \text{(D24)}$$

For the cases of interest in this report, the denominator D always turns out to be positive. Thus the sign of dP/ds is governed by the sign of N. For $N \leq 0$, seeding does not improve the power density.

APPENDIX E

DETAILS OF THE CALCULATION

The break-even condition (eq. (23)) is rewritten as

$$\beta_e\beta_i\left\{\frac{T_e}{T_e - T} + \Psi\left[(1 - x_c)\left(3 + \frac{2eV_c}{kT_e} + \frac{T_e}{T_e - T}\right) + \frac{T_e}{T_e - T}\right]\right.$$

$$\left. + x_c\left(3 + \frac{2eV_c}{kT_e} + \frac{T_e}{T_e - T}\right) + \left(1 - \frac{m_c}{m_s}\right)(1 - 2x_c)\left(\frac{3}{2} + \frac{eV_c}{kT_e}\right)\frac{\nu_{ei}}{\nu_e}\right\}$$

$$= 3\,\frac{\nu_{ei}}{\nu_e} - \frac{\nu_{ec}}{\nu_e}\left[2n + 1 + \frac{T_e}{T_e - T} - x_c\left(3 + \frac{2eV_c}{kT_e} + \frac{T_e}{T_e - T}\right)\right]$$

$$- \left(1 - \frac{m_c}{m_s}\right)\frac{\nu_{ei}}{\nu_e}\left\{3\left(1 - \frac{x_c}{2}\right)\frac{\nu_{ei}}{\nu_e} + \frac{\nu_{ec}}{\nu_e}\left[\frac{3}{2} + \frac{eV_c}{kT_e} - \left(1 - \frac{x_c}{2}\right)(2n + 1)\right]\right\} \qquad \text{(E1)}$$

where the magnetic field B enters only through $\beta_e\beta_i$, which for $s = 0$ becomes

$$\beta_e\beta_i = \left(\frac{eB}{m_e\nu_e}\right)\left(\frac{2eB}{m_c\nu_{c+c}}\right) \qquad \text{(E2)}$$

The expressions for ν_{ec}/ν_e and ν_{ei}/ν_e in the limit $s = 0$ are obtained from equations (D8) and (D10)

$$\frac{\nu_{ec}}{\nu_e} = \frac{(1 - x_c)Q_{ec}}{(1 - x_c)Q_{ec} + x_cQ_{ei}} \qquad \text{(E3)}$$

$$\frac{\nu_{ei}}{\nu_e} = \frac{x_cQ_{ei}}{(1 - x_c)Q_{ec} + x_cQ_{ei}} \qquad \text{(E4)}$$

where from equations (C19) and (C20)

$$Q_{ei} = 4.34\times10^{-18} \frac{\ln \Lambda}{\left(\frac{kT_e}{e}\right)^2} \quad \text{(sq m)} \tag{E5}$$

$$\Lambda = 1.55\times10^{13} \frac{1}{N_i^{1/2}} \left(\frac{kT_e}{e}\right)^{3/2} \tag{E6}$$

and the limit of zero seed

$$N_i = x_c N_c^o \tag{E7}$$

The degree of ionization x_c of the carrier gas is calculated from equation (19), which for $s = 0$ becomes

$$\frac{x_c^2}{1 - x_c} = \frac{6.04\times10^{27}}{N_c^o} \left(\frac{g_{c+}}{g_c}\right)\left(\frac{kT_e}{e}\right)^{3/2} \exp\left(-\frac{eV_c}{kT_e}\right) \tag{E8}$$

When $x_c \ll 1$, a good approximation to x_c is

$$x_c = \frac{g(T_e)}{\left(N_c^o\right)^{1/2}} = \frac{7.77\times10^{13}}{\left(N_c^o\right)^{1/2}} \left(\frac{g_{c+}}{g_c}\right)^{1/2} \left(\frac{kT_e}{e}\right)^{3/4} \exp\left(-\frac{eV_c}{2kT_e}\right) \tag{E9}$$

Finally, the ingredients will be assembled for the quantity Ψ, which was defined in equation (D18). The quantities R_{s+c} and R_{c+c} for ion-atom collisions are calculated from data on ion mobilities. From the definition (D13) of R_{rt} and equations (C28) and (C29), it follows that

$$R_{rt} = \frac{e}{\mu_{rt} N_t} = \frac{e}{(\mu_0)_{rt} N_0} \tag{E10}$$

where $N_0 = 2.69\times10^{25}$ atoms per cubic meter is the standard gas density and $(\mu_0)_{rt}$ the corresponding mobility. If μ_0 is given in square centimeters per volt per second, as is usually the case,

$$R_{rt} = 5.96\times10^{-41}\ \frac{1}{(\mu_0)_{rt}} \tag{E11}$$

For collisions between ions of species A^+ and B^+, equations (C9) and (C10) give

$$\nu_{A^+B^+} = N_{B^+}Q_{ii}\left(\frac{8kT}{\pi m_{A^+B^+}}\right)^{1/2} \tag{E12}$$

if it is assumed that both ion species are at the temperature T of the gas. When equation (E12) and the expression for Q_{ii} (eq. (C23)) are substituted into the definition for the ion-ion collision coefficient $R_{A^+B^+}$ (eq. (D13)), the following expression is obtained:

$$R_{A^+B^+} = 1.38\times10^{-27}\ m_{A^+B^+}^{1/2}\frac{\ln(\Lambda'^2 + 1)}{\left(\frac{kT}{e}\right)^{3/2}} \tag{E13}$$

where

$$\Lambda' \approx \left(\frac{T}{T_e}\right)^{3/2}\Lambda \tag{E14}$$

Then Ψ may be written

$$\Psi = \left[\frac{(\mu_0)_{c^+c}}{(\mu_0)_{s^+c}} - 1\right]\frac{1 + r}{\frac{(\mu_0)_{c^+c}}{(\mu_0)_{s^+c}} + r} \tag{E15}$$

where

$$r = \frac{x_c}{1 - x_c}\frac{R_{s^+c^+}}{R_{c^+c}} = 0.945(\mu_0)_{c^+c}\sqrt{\frac{A_cA_s}{A_c + A_s}}\ \frac{x_c}{1 - x_c}\ \frac{\ln(\Lambda'^2 + 1)}{\left(\frac{kT}{e}\right)^{3/2}} \tag{E16}$$

and A_c and A_s are the atomic weights of carrier gas and seed, respectively. The units of $(\mu_0)_{c^+c}$ are square centimeters per volt per second in equation (E16). Note

TABLE II. - PROPERTIES OF NOBLE GASES

Gas	Atomic weight of carrier gas, A_c	Ionization potential, V_c, eV	Ground state statistical weight of carrier gas -		Ion mobility at 300° K and gas density of 2.69×10^{19} atoms per cubic centimeter (refs. 12 and 14), μ_0, sq cm/(V)(sec)
			Atom, g_c	Ion, g_{c^+}	
Helium	4.003	24.580	1	2	10.8
Neon	20.183	21.559	1	6	4.2
Argon	39.944	15.755	1	6	1.60
Krypton	83.80	13.996	1	6	.90
Xenon	131.30	12.127	1	6	.58

TABLE III. - ATOMIC WEIGHTS AND MOBILITIES

OF ALKALI SEED IONS IN NOBLE GASES

[Mobility data taken from table 9-2-2 of ref. 12.]

Seed	Atomic weight of seed, A_s	Background gas				
		Helium	Neon	Argon	Krypton	Xenon
		Ion mobility at 290° K and gas density of 2.69×10^{19} atoms per cubic centimeter, μ_0, sq cm/(V)(sec)				
Lithium	6.94	24.4	11.1	4.7	3.7	2.8
Sodium	22.991	22.8	8.2	3.0	2.2	1.7
Potassium	39.100	21.6	7.6	2.6	1.9	1.4
Rubidium	85.48	20.2	6.8	2.2	1.5	1.0
Cesium	132.91	18.5	6.1	2.1	1.3	.91

that Ψ vanishes when the mobilities of the seed and carrier gas ions are equal.

With the previous expressions it is a simple matter to calculate $\beta_e\beta_i$ from equation (E1) for prescribed values of T_e, T, and N_c^o. Then the corresponding value of B is calculated from equation (E2), which upon insertion of the expression for ν_{c+c} in terms of μ_{c+c} (eq. (C28)) and the relation between μ_{c+c} and the standard mobility $(\mu_0)_{c+c}$ (eq. (C29)) becomes

$$B^2 = 2.12\times10^{-33}\frac{(1 - x_c)N_c^o\nu_e\beta_e\beta_i}{(\mu_0)_{c+c}} \tag{E17}$$

$$\nu_e = 6.69\times10^5 \left(\frac{kT_e}{e}\right)^{1/2} \left[(1 - x_c)Q_{ec} + x_c Q_{ei}\right] N_c^o \tag{E18}$$

The gas velocity required to attain the prescribed electron temperature is calculated from equation (24), which may be written

$$uB(1 - K) = \frac{8.98\times10^{-10}}{A_c^{1/2}} (1 + \beta_e\beta_i)\nu_e(T_e - T)^{1/2} \tag{E19}$$

The pertinent properties of the rare gases are summarized in table II. Table III gives the atomic weights and mobilities of the alkali seed ions in the noble gases. The mobilities of the alkali ions in the noble gases are well predicted by classical collision theory in which the interaction of the ion and atom is assumed to be a polarization attraction (ref. 12). In this case the theoretical mobility is independent of gas temperature, as will be assumed here. The available experimental data (ref. 13) indicate that this is a reasonably good assumption. The mobility of the noble gas ions in their parent gases, however, decreases slowly with increasing temperature because of the effect of charge exchange (ref. 14). The following theoretical expressions for the temperature dependence are given in reference 14 and are in good agreement with experiment:

$$\frac{1}{\mu_0} (He^+ \text{ in } He) = 2.96\times10^{-3}\, T^{1/2} + 3.11\times10^{-2} + 2.11\times10^{-2}\, T^{-1} + 6.66\, T^{-2} \tag{E20a}$$

$$\frac{1}{\mu_0} (Ne^+ \text{ in } Ne) = 8.69\times10^{-3}\, T^{1/2} + 9.16\times10^{-2} + 0.20\, T^{-1} + 59.7\, T^{-2} \tag{E20b}$$

$$\frac{1}{\mu_0} (Ar^+ \text{ in } Ar) = 2.08\times10^{-2}\, T^{1/2} + 0.24 + 1.33\, T^{-1} + 1.43\times10^{2}\, T^{-2} \tag{E20c}$$

These expressions, which are claimed to be valid for 50^o to 1200^o K, are used in the calculations. Unfortunately, no expression for the temperature dependence of xenon was given. For xenon the same temperature dependence as for argon is assumed (eq. (E20c)), but with the constant 0.24 replaced by 1.36 in order to give the correct value of μ_0 at 300^o K.

To illustrate the procedure, a sample calculation for argon seeded with cesium (atomic weight = 132.91) is given. An electron temperature $T_e = 8000^o$ K (0.689 ev)

and a gas temperature of $T = 500^{o}$ K are chosen. First the break-even point for zero ion slip is determined from equation (31). From equation (E9)

$$g(T_e) = 7.77\times10^{13}\sqrt{6}\,(0.689)^{3/4}\exp\left[-\frac{15.755}{2(0.689)}\right] = 1.57\times10^{9}$$

Let $\ln\Lambda = 7.0$ as a first approximation. Then from equation (E5)

$$Q_{ei} = \frac{(4.34\times10^{-18})7.0}{(0.689)^2} = 6.40\times10^{-17} \qquad \text{(sq m)}$$

The electron-atom cross section for argon at this temperature is $Q_{ec} = 4.25\times10^{-20}$ square meter, so that $Q_{ec}/Q_{ei} = 0.664\times10^{-3}$. The coefficients of equation (28) are $a = 4.33$, $b = 16.06$, $c = 0.935$ (for $n = 1.13$), and from equation (30) $(\nu_{ec}/\nu_{ei})_{lim} = 0.0582$. The limiting gas density is from equation (31) $(N_c^o)_{lim} = 1.895\times10^{22}\,m^{-3}$, and for this gas density equation (E6) gives $\ln\Lambda = 6.40$. The calculation is repeated with this new value of $\ln\Lambda$. The ratio $(\nu_{ec}/\nu_{ei})_{lim}$ is essentially unchanged, while the new value of N_c^o is 1.582×10^{22}, for which $\ln\Lambda = 6.44$. Another iteration gives $(N_c^o)_{lim} = 1.60\times10^{22}$ and $\ln\Lambda = 6.45$, and further iterations are not required.

The value of $(N_c^o)_{lim}$ determines the point where $\beta_e\beta_i = 0$. For other gas densities, $\beta_e\beta_i$ is calculated from equation (E1). For $N_c^o < (N_c^o)_{lim}$, both sides of equation (E1) are positive. For $N_c^o > (N_c^o)_{lim}$, the right side of equation (E1) is negative, but as the gas density is increased, the coefficient of the left side changes from positive to negative. In the present example, this occurs at $N_c^o = 4.69\times10^{22}$ per cubic meter. Since $\beta_e\beta_i$ must be positive, for the range of densities $1.6\times10^{22} < N_c^o < 4.69\times10^{22}$ the break-even condition cannot be satisfied; hence seed increases the power. For $N_c^o > 4.69\times10^{22}$, the coefficient on the left side of equation (E1) is negative, and a positive value of $\beta_e\beta_i$ may be found that satisfies the equality. Figure 18(a) shows the variation of $\beta_e\beta_i$ with N_c^o.

The sign of dP/ds in regions off the break-even curve is determined from equation (23) as follows. If both the right and left sides of equation (23) are positive and if $\beta_e\beta_i$ is smaller than its break-even value (determined from eq. (E1)), then inequality (23) is satisfied and $dP/ds < 0$. If $\beta_e\beta_i$ is larger than its break-even value, the inequality cannot be satisfied and $dP/ds > 0$. Therefore, in figure 18(a) dP/ds is positive above the left branch of the break-even curve and negative below the curve. When both the left and right sides of equation (23) are negative, as in the present example for $N_c^o > 4.69\times10^{22}$, then for $\beta_e\beta_i < (\beta_e\beta_i)_{break\text{-}even}$ the inequality is not satisfied and

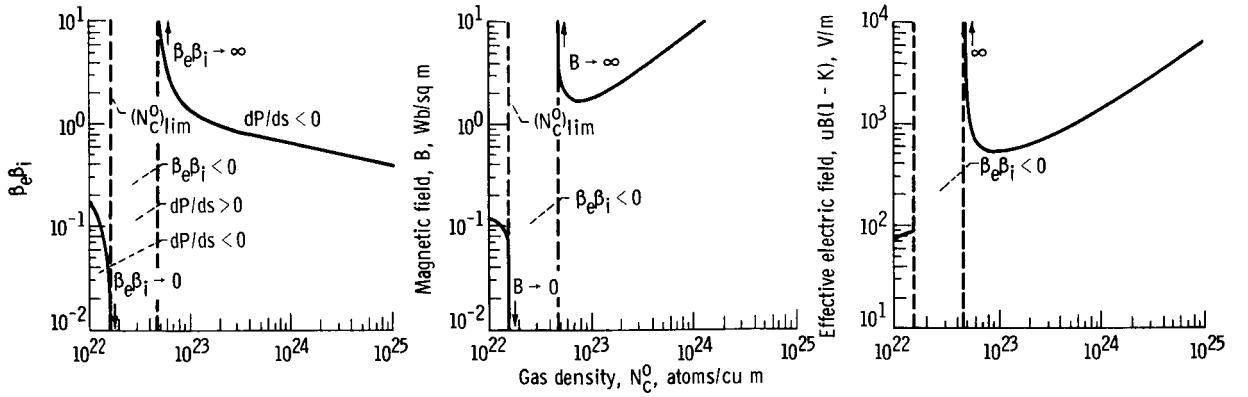

(a) $\beta_e\beta_i$ against gas density.

(b) Magnetic field against gas density.

(c) Effective electric field against gas density.

Figure 18. - Results of sample calculation for cesium-seeded argon. Electron temperature, 8000° K; gas temperature, 500° K.

$dP/ds > 0$. In the region $1.6\times10^{22} < N_c^o < 4.69\times10^{22}$, $dP/ds > 0$, as mentioned previously.

Once $\beta_e\beta_i$ has been calculated for assigned values of N_c^o, T_e, and T, the corresponding values of the magnetic field B and the effective electric field uB(1 - K) are obtained from equations (E17) and (E19), respectively. The results for the example are shown in figures 18(b) and (c). From figure 18(b) the values of N_c^o corresponding to a particular magnetic field may be picked off; for example, for B = 2 webers per square meter, N_c^o is 5.8×10^{22} and 1.15×10^{23} per cubic meter. The values of uB(1 - K) at these densities are read from figure 18(c) and are 7.3×10^{2} and 5.25×10^{2} volts per meter, respectively. These two points lie on the lower branch of the break-even curve of figure 4(b). Curves similar to those of figures 18(b) and (c) are constructed for each assigned electron temperature, and the densities N_c^o and the electric field uB(1 - K) are read from the curves for a specified magnetic field. The results for cesium-seeded argon are plotted in figure 4 for various magnetic fields. At high electron temperatures (above 9000° K), points on the upper branches of the break-even curves of figure 4 are obtained.

REFERENCES

1. Kerrebrock, Jack L.: Conduction in Gases with Elevated Electron Temperature. Engineering Aspects of Magnetohydrodynamics, C. Mannal and N. W. Mather, eds., Columbia Univ. Press, 1962, pp. 327-346.

2. Ben Daniel, D. J.; and Tamor, S.: Nonequilibrium Ionization in Magnetohydrodynamic Generators. Rep. 62-RL-(2922-E), General Electric Co., Jan. 1962.

3. Hurwitz, H., Jr.; Sutton, G. W.; and Tamor, S.: Electron Heating in Magnetohydrodynamic Power Generators. ARS Jour., vol. 32, no. 8, Aug. 1962, pp. 1237-1243.

4. Lyman, Frederic A.; Goldstein, Arthur W.; and Heighway, John E.: Effect of Seeding and Ion Slip on Electron Heating in a Magnetohydrodynamic Generator. NASA TN D-2118, 1964.

5. Heighway, John E.; Nichols, Lester D.: Brayton Cycle Magnetohydrodynamic Power Generation with Nonequilibrium Conductivity. NASA TN D-2651, 1965.

6. Burgers, J. M.: Selected Topics from the Theory of Gas Flow at High Temperatures. Ch. V. The Application of Transfer Equations to the Calculation of Diffusion, Heat Conduction, Viscosity and Electric Conductivity. Tech. Notes BN-124a, b, Inst. Fluid Dynamics and Appl. Math., Univ. of Maryland, May 1958.

7. Burgers, J. M.: Statistical Plasma Mechanics. Ch. 5 of Symposium on Plasma Dynamics, F. H. Clauser, ed., Addison-Wesley Pub. Co., Inc., 1960.

8. Burgers, J. M.: Some Problems of Magneto-Gasdynamics. Lectures on Fluid Mech., by Sydney Goldstein, Intersci. Pub., Inc., 1960, p. 293.

9. Spitzer, Lyman, Jr.: Physics of Fully Ionized Gases. Second ed., Intersci. Pub., Inc., 1962, p. 127.

10. Delcroix, J. L.: Introduction to the Theory of Ionized Gases. Intersci. Pub., Inc., 1960, p. 125.

11. Brown, Sanborn C.: Basic Data of Plasma Physics. Tech. Press, M.I.T., 1959.

12. McDaniel, E. W.: Collision Phenomena in Ionized Gases. John Wiley & Sons, Inc., 1964, ch. 9.

13. Dalgarno, A.: Diffusion and Mobilities. Atomic and Molecular Processes, ch. 16, D. R. Bates, ed., Academic Press, 1962, p. 654.

14. Chanin, Lorne M.; and Biondi, Manfred A.: Temperature Dependence of Ion Mobilities in Helium, Neon, and Argon. Phys. Rev. vol. 106, no. 3, May 1, 1957, pp. 473-479.